Mon. Not. R. Astron. Soc. **000**, 1–?? (2011) Printed 14 October 2013 (MN LATEX style file v2.2)

Photometric properties of intermediate redshift Type Ia Supernovae observed by SDSS-II Supernova Survey

N. Takanashi[1⋆], M. Doi[2,3], N. Yasuda[3], K. Konishi[4], D. P. Schneider[5,6], D. Cinabro[7], J. Marriner[8], H. Kuncarayakti[9]

[1] *Institute of Industrial Science, The University of Tokyo, 4-6-1 Komaba, Meguro-ku, Tokyo 153-8505, Japan.*
[2] *Institute of Astronomy, Graduate School of Science, The University of Tokyo, 2-21-1 Osawa, Mitaka, Tokyo 181-0015, Japan.*
[3] *Kavli Institute for the Physics and Mathematics of the Universe, The University of Tokyo, 5-1-5 Kashiwanoha, Kashiwa, Chiba 277-8568, Japan.*
[4] *Nikon Corporation, 201-9 Miizugahara, Kumagaya, Saitama 360-8559, Japan.*
[5] *Department of Astronomy and Astrophysics, The Pennsylvania State University, University Park, PA 16802, USA.*
[6] *Institute for Gravitation and the Cosmos, The Pennsylvania State University, University Park, PA 16802, USA.*
[7] *Department of Physics and Astronomy, Wayne State University, Detroit, MI 48202, USA.*
[8] *Center for Particle Astrophysics, Fermi National Accelerator Laboratory, Batavia, IL 60510, USA.*
[9] *Departamento de Astronom?a, Universidad de Chile, Casilla 36-D, Santiago, Chile.*

14 October 2013

ABSTRACT

We have analyzed the *u-*, *g-*, *r-*, *i-* and *z*-band light curves of 342 intermediate redshift (z $<$ 0.24) type Ia supernovae (SNe Ia) with normal spectra observed by the Sloan Digital Sky Survey-II Supernova Survey (SDSS-II SN Survey). The multi-band light curves were parameterized into rest-frame *U-*, *B-*, *V-*, *R-* and *I*-band stretch factors, peak luminosities, and the *B*-band maximum luminosity dates using the Multi-band Stretch Method. Stretch-magnitude and stretch-colour relations of the SDSS SNe Ia are similar to those of nearby SNe Ia. We found that most of the SNe Ia which appeared in red host galaxies ($u - r > 2.5$) have a narrow light curve and the SNe Ia which appeared in blue host galaxies ($u - r < 2.0$) have a variety of light curve widths. We infer that "tardy" SNe Ia, whose rate is proportional to the total stellar mass and possibly related to an old progenitor, appeared in both the red and blue host galaxies but "prompt" SNe Ia, whose rate is proportional to the star formation rate and is possibly related to a young progenitor, appeared in only the blue host galaxies; both types have a small dispersion (< 0.10 mag) in colour excess. The Kolmogorov-Smirnov test shows that the colour distribution of SNe Ia with a medium light curve width depends upon host galaxy colour (significance level 96.2%). These results indicate that there may be two types of SNe Ia with different intrinsic colours. We also discuss dust properties of host galaxies based on colours and magnitudes of SNe Ia and find supportive evidence that there may be two kinds of dust with different extinction properties.

Key words: supernova: general. - light curve. - dust property.

1 INTRODUCTION

Type Ia supernovae (SNe Ia) are known as excellent standard candles for tracing the expansion history of the Universe because of their homogeneity and high luminosity (Filippenko 2005). Since the early 1990s, several SN Ia search programs which aimed to measure the Hubble constant have been performed. The CALAN/TOLOLO Supernova Search, started in 1990 (Hamuy et al. 1993; Phillips 1993; Hamuy et al. 1995), succeeded in producing a moderately distant ($0.01 < z < 0.10$) sample of SN Ia. The Supernova Cosmology Project (SCP) and the High-Z Team (HZT) are independent high redshift ($z \sim 0.5$) SN searches designed to measure the cosmological parameters of the Universe.

After a careful analysis of their observed SNe Ia, both SCP and HZT reported the accelerating expansion of the Universe (Riess et al. 1998; Schmidt et al. 1998; Perlmutter et al. 1999). This result implies that there is an unknown

⋆ E-mail: naohiro.takanashi@emp.u-tokyo.ac.jp

component in the Universe, named "dark energy" (Huterer et al. 1998; Turner 1999). The idea of dark energy has also been supported by studies of cosmic microwave background (CMB) fluctuations (e.g. Spergel et al. 2007; Komatsu et al. 2011), baryon acoustic oscillations (BAO, e.g. Percival et al. 2010; Anderson et al. 2012; Samushia et al. 2013), large scale structure (e.g. Tegmark et al. 2006; Reid et al. 2010; Benson et al. 2013) and gravitational lensing (e.g. Oguri et al. 2008; Li et al. 2009; Oguri et al. 2012). In addition, a most recent result based on CMB analysis has been obtained by the orbiting Planck satellite (Planck Collaboration et al. 2013), supporting the standard ΛCDM cosmology with improved measurements.

Cosmological studies with SNe Ia have been continued and refined, with several new SN search programs; for example, the Lick Observatory and Tenagra Observatory Supernova Searches (LOTOSS, Filippenko et al. 2001), the Carnegie Supernova Program (CSP, Hamuy et al. 2006), the Texas Supernova Search (Quimby et al. 2005), the Nearby Supernova Factory (SNfactory, Aldering et al. 2002), the CfA Supernova Group (CfA3, Hicken et al. 2009a), the Sloan Digital Sky Survey-II Supernova Survey (SDSS-II SN Survey, Frieman et al. 2008), the Equation of State: SupErNovae trace Cosmic Expansion project (ESSENCE, Wood-Vasey et al. 2007), the CHilean Automatic Supernova sEarch (CHASE, Pignata et al. 2009), and the SuperNova Legacy Survey (SNLS, Pritchet et al. 2005; Guy et al. 2010). The data from these groups combine to make a large sample of SNe Ia with high quality photometry and spectroscopy at various redshifts in order to reduce random errors and to control systematic effects which affect measurements of the cosmological parameters (e.g Tonry et al. 2003; Knop et al. 2003; Riess et al. 2004; Astier et al. 2006; Wood-Vasey et al. 2007; Kowalski et al. 2008; Amanullah et al. 2010; Conley et al. 2011; Suzuki et al. 2012; Campbell et al. 2013).

As described above, SNe Ia show properties which are more homogeneous than those of any other astronomical objects which can be used as standard candles at cosmological distances. However, many studies have also revealed an intrinsic diversity of SN Ia properties. For example, there are several subgroups of SNe Ia which are classified by spectral features. SN1991T-type and SN1991bg-type are well documented subgroups of SNe Ia (Branch et al. 1993; Nugent et al. 1995). The SN1991T-type SN Ia has a slightly broader light curve and brighter peak magnitude than a normal SN Ia (Phillips et al. 1992). The SN1991bg-type SN Ia has a narrower light curve and fainter peak magnitude than a normal SN Ia (Filippenko 1989; Leibundgut et al. 1993). Other subtypes of SNe Ia have also been described, such as the ".Ia" explosions (Bildsten et al. 2007), which are only about one-tenth as bright as SN Ia, and the SNe Iax (Foley et al. 2013), which are generally similar to the characteristics of a SN Ia but with some different properties as seen on SN 2002cx, the prototypical member of this subclass.

We can also find intrinsic diversity in spectra of SNe Ia without including any obviously SN1991T-like and SN1991bg-like SNe (e.g. Benetti et al. 2005). Recent studies have reported that even the spectroscopically normal SN Ia (called "Branch normal", Branch et al. 1993) may have subgroups. Mannucci et al. (2005), in order to describe the observed SN Ia rate, proposed that the population of SNe Ia consists of two components, one named "prompt", whose rate is proportional to the star formation rate and is possibly related to a young progenitor, and the other named "tardy", whose rate is proportional to the total stellar mass and is possibly related to an old progenitor (see also Scannapieco et al. 2005; Mannucci et al. 2006). Based on photometric and spectroscopic observations of SN2005hj, Quimby et al. (2007) suggested that there may be two subgroups within Branch normal SNe Ia produced by two different progenitor channels. Ellis et al. (2008) reported that rest frame ultraviolet spectra of SNe Ia have significant variation using a sample of 36 events at intermediate redshift ($z = 0.5$).

Recent studies with large SN Ia samples, from low redshift to high redshift, show a significant correlation between SNe Ia properties and their host galaxies. Using a local SNe Ia sample, Kelly et al. (2010) showed that SNe Ia occurring in physically larger, more massive hosts are $\sim$ 10% brighter after light curve correction. Hicken et al. (2009b) demonstrated from CfA3 data that SNe Ia which appeared in Scd/Sd/Irr hosts and E/S0 hosts may arise from different populations (see also Neill et al. 2009). Sullivan et al. (2010) showed SNe Ia properties depend on the global characteristics of their host galaxies from SNLS and other data. Lampeitl et al. (2010b) confirmed the effect of host galaxies on SNe Ia in the SDSS-II SN Survey. Also using data from the SDSS-II SN Survey, Smith et al. (2012) found that the rate of SN Ia per unit stellar mass is much higher in star-forming host galaxies compared to passive ones, and Galbany et al. (2012) suggested that SNe that exploded at large distances from their elliptical hosts tend to have narrower light curves.

Takanashi et al. (2008) (hereafter, TAK08) presented photometric properties of 108 nearby ($z \sim 0.1$) SNe Ia. In this study, we investigate photometric properties of SNe Ia at intermediate redshift ($z \sim 0.2$). We use data obtained by the SDSS-II SN Survey (York et al. 2000; Frieman et al. 2008), which is well calibrated, homogeneous and the first large SN Ia sample at an intermediate redshift. The SDSS-II SN Survey is a SN survey with the wide-field SDSS 2.5-m telescope (Gunn et al. 2006) and wide-field imaging camera (Gunn et al. 1998) at Apache Point Observatory (APO) operated by an international collaboration. The SDSS-II SN Survey complements existing ground-based low redshift (LOTOSS, SNfactory, CSP etc.) and high redshift (ESSENCE, SNLS) SN search programs. Through repeated scans of the SDSS southern equatorial stripe (82N and 82S, about 2.5 deg wide by 120 deg long) every other night over the course of three 3-month campaigns (Sept-Nov. 2005-7), the SDSS-II SN Survey obtained well-measured, densely sampled *u-, g-, r-, i-* and *z*-band light curves (Holtzman et al. 2008).

Zheng et al. (2008) presented spectroscopy of SNe found in the first season of the SDSS-II SN Survey, and Kessler et al. (2009) reported measurements of the Hubble diagram of SNe Ia discovered during the first season.

In this paper, we present photometric properties of the SDSS SNe Ia parameterized by the Multi-band Stretch Method (TAK08). In particular, we focus on the stretch distribution of the SDSS SNe Ia and the relationship between a stretch factor and photometric properties. We first provide information about the data used in this work (§2), then describe how we parameterize the multi-band light curves (§3). The observational selection biases expected in the SDSS SNe Ia are discussed (§4), and we show photometric properties of

the SDSS SNe Ia, comparing them with those of nearby SN samples from the literature (§5.1). We also examine properties of host galaxy dust (§5.2).

The SNe Ia which were reported to the International Astronomical Union (IAU) have a SN ID like SN2005eg. However, there are many SNe Ia (most without spectroscopic typing configuration) that were not reported to the IAU in the SDSS sample used in this study. We use a SDSS SN ID like SDSS-SN12345 for the name of those SNe without IAU designations in this paper.

2 PHOTOMETRIC DATA

We analyzed *u-, g-, r-, i-* and *z*-band (Fukugita et al. 1996) light curves of 643 SNe Ia obtained by the 2005-2007 SDSS-II SN Survey. As we show in Table 1, the SNe Ia sample (hereafter SDSS sample) consists of four groups, which are (1) spectroscopically confirmed SNe Ia (we call them type "120"), (2) spectroscopically probable SNe Ia (type "119"), (3) SNe Ia spectroscopically identified by observers outside the SDSS (type "118") and (4) photometrically probable SNe Ia with host galaxy spectroscopic redshifts (type "105") which are identified as SNe Ia based on luminosity, colour, and light curve shapes (see details in Sako et al. 2008). We do not include known peculiar SNe Ia classified by Zheng et al. (2008) in the sample (SN2005js, SN2005gj, SDSS-SN7017, and SN2005hk are excluded). We do not use the SNe Ia whose photometry is not based upon the SDSS calibration stars in the same frame in order to avoid photometric uncertainty. Since we assigned higher priority of spectroscopic observations to colour selected SN Ia candidates, spectroscopically observed SNe Ia (type-120, 119) are biased to blue and normal SNe Ia. To reduce the selection effect, we include type-105 SNe Ia in this study. Note that the type-105 SNe Ia are not spectroscopically confirmed as SNe Ia.

Figure 1 shows the redshift distribution of the SDSS sample used in this study. The redshifts of all SNe of the in the sample are measured by spectroscopic observations of their host galaxies or SN spectra. The average redshift is $z \sim 0.22$, and about 70% of samples lies in the range $0.1 < z < 0.3$. Because of insufficient telescope time for spectroscopic observations of faint objects, we did not obtain spectra for many SNe Ia, especially those at higher redshift. We did acquire light curves of many of those missed "SNe Ia", but we use only light curves which are classified as having a high probability of being a SN Ia (the type-105 SN Ia of Sako et al. 2008). As is apparent in Figure 1, the SDSS sample is strongly biased at higher redshifts. In order to reduce the effect of bias, we use only 342 SNe Ia in the range $z < 0.24$ (see §5.1).

The photometry of the SNe Ia was mainly obtained by the SDSS camera on the 2.5-m telescope at APO. The flux of each SNe Ia has been measured by Holtzman et al. (2008) with the technique named "Scene Modeling Photometry (SMP)". SMP does not use a template-subtracted image for photometry. The technique fits all of the individual reduced frames with a model of the galaxy background and the SN, and measures the flux from the model. The model of each image is generated from the sum of a set of stars, a galaxy, a SN, and background. As a result, SMP can avoid degrading the PSF and any spatial resampling that leads to correlated noise between pixels. The basic concept is similar to the technique of SNLS (Astier et al. 2006).

Table 2. Synthetic AB magnitude of Vega in the SDSS filters.

u	*g*	*r*	*i*	*z*
0.951	-0.080	0.169	0.389	0.556

Calculated from the STSDAS v3.3 synphot Vega spectrum assuming V=+0.03.

In order to discuss properties of the SDSS sample, we use the nearby SNe Ia sample (hereafter Nearby sample) from TAK08. The Nearby sample includes 108 SNe Ia in the range $z < 0.11$ with *U-, B-, V-, R-* and *I*-band light curves. The light curves were parameterized by the Multi-band Stretch Method and the parameters are listed in Table 2 of TAK08.

3 ANALYSIS

We applied the Multi-band Stretch Method (TAK08) to the light curves in five passbands. We fit up to 11 parameters to each event: *U-, B-, V-, R-* and *I*-band stretch factors, *U-, B-, V-, R-* and *I*-band peak magnitudes, and a time t_{Bmax} for maximum light in the *B*-band. The method does not include any dust / colour corrections and has the advantage that we can simply parameterize the light curve shape and luminosity without any assumptions. We used the *U-, B-, V-, R-* and *I*-band light curve templates which are adjusted to coincide with a SN Ia with $s_{(B)} = 1.0$ SED template (Nugent et al. 2002) for the light curve fitting. We derived absolute magnitudes for the SDSS sample using redshifts under the assumption of the standard cosmological parameters ($H_0 = 70.8$ km/s/Mpc, $\Omega_M = 0.262, \Omega_\Lambda = 0.738$ from Spergel et al. 2007). We corrected extinction by dust in the Milky Way according to Schlegel et al. (1998). The differences from the analysis in TAK08 are that (1) we need to transform the photometric data from the native SDSS system to the Vega system, and (2) we must apply cross filter K-corrections to the data. We describe these procedures below.

3.1 Magnitude System

The SMP data are provided in the natural system of the SDSS 2.5-metre telescope (Doi et al. 2010). We need to transform this ugriz data to the Vega system to compare SDSS photometry with *U-, B-, V-, R-* and *I*-band light curves of the Nearby sample. We transformed the data in the following way.

First, the native SDSS system was transformed into the AB system (J. Marriner, private communication).

$$\begin{aligned} u(AB) &= u(SDSS) - 0.065 \\ g(AB) &= g(SDSS) + 0.022 \\ r(AB) &= r(SDSS) + 0.007 \\ i(AB) &= i(SDSS) + 0.022 \\ z(AB) &= z(SDSS) + 0.016 \end{aligned}$$

Table 1. Type and properties of the SDSS SNe Ia. The numbers in parentheses are the number of SNe Ia we used in discussion after §5.

Type	Number	Average Redshift	Comment
all	643 (342)	0.22	
120	425 (246)	0.21	
119	45 (19)	0.24	
118	7 (2)	0.13	SN2005hj, SN2006eq, SN2006fz, SN2007fr, SN2007ht, SN2007lu, SN2007lw
105	169 (75)	0.23	Selected by Sako et al. (2008)

type-120 is a spectroscopically confirmed SN Ia
type-119 is a spectroscopically probable SN Ia
type-118 is a SN Ia identified by external groups of SDSS
type-105 is a photometrically probable SN Ia with spectroscopic redshift of the host galaxy

Next, the AB system was transformed into the Vega system. To adjust zeropoints of the AB system and the Vega system, the *u-, g-, r-, i-* and *z*-band magnitude of Vega in the AB system (Table 2) were added as follows.

$$\begin{aligned} u(Vega) &= u(AB) - u(AB)_{Vega} \\ g(Vega) &= g(AB) - g(AB)_{Vega} \\ r(Vega) &= r(AB) - r(AB)_{Vega} \\ i(Vega) &= i(AB) - i(AB)_{Vega} \\ z(Vega) &= z(AB) - z(AB)_{Vega} \end{aligned}$$

At the end of this procedure, we have transformed the *u-, g-, r-, i-* and *z*-band magnitudes of our supernovae into the Vega system.

3.2 Cross-Filter K-correction

The next step is to apply K-corrections to transform observed *u-, g-, r-, i-* and *z*-band magnitudes to *U-, B-, V-, R-* and *I*-band magnitudes (see Figure 2). We have to choose an appropriate filter combination for each cross-filter K-correction as a function of redshift. In this study, we transformed (*u, g, r, i*) → (*U, B, R, I*) in the range $z \leqslant 0.05$, (*u, g, r, i, z*) → (*U, B, V, R, I*) in the range $0.05 < z \leqslant 0.24$, and (*g, r, i, z*) → (*U, B, V, R*) in the range $0.24 < z \leqslant 0.50$. The cross-filter K-correction was applied according to the following definition.

$$\begin{aligned} K_{XY,t}^{counts} &= ZP_Y - ZP_X + 2.5\log(1+z) \\ &\quad +2.5\log\frac{\int \lambda F(\lambda,t) S_X(\lambda) d\lambda}{\int \lambda F[\lambda/(1+z),t] S_Y(\lambda) d\lambda} \end{aligned} \quad (1)$$

Here ZP_X is the zeropoint of X-band in the magnitude system, $F(\lambda, t)$ is the spectral energy distribution (SED) of the SN Ia at time t, $S_X(\lambda)$ is the effective response of the X-band filter, and $K_{XY,t}$ is the value of K-correction from the X-band to the Y-band at time t. We use the spectrum of Hsiao et al. (2007) for the K-correction. Ideally, we should apply a spectrum template based on the proper type of each SN Ia (e.g. SN1991T-like, SN1991bg-like) for K-corrections, but we applied Hsiao's template all SNe Ia. The template is warped to fit the observed ugriz photometry. We use the standard galactic extinction curve (Cardelli et al. 1989) for warping.

Since we have calibrated the flux with only the cross-filter K-correction, we should also apply the stretch K-correction. As we have noted above, we chose the appropriate filter combination for the cross-filter K-correction as a function of redshift, but the K-corrected bandpass of observed band is not the same as that of rest frame *B*-band. We should correct the difference of stretch factors due to the different bandpass. We use the relations between $s_{(B)}$ and the stretch factors of other bands derived from the Nearby SNe Ia (Table 3) for the stretch K-correction. Based on those relations, we calculated the size of the stretch K-correction by interpolating stretch factors of different two bands. Figure 3 shows the size of stretch corrections of the SDSS SNe Ia versus redshift. We show the typical size of the stretch correction of the SN Ia with $s_{(B)} = 1.0$ as a solid line. The correction becomes smallest at the redshift where the K-corrected bandpass of observed band agrees well with that of rest frame *B*-band. For the SDSS SNe Ia, the correction reaches a maximum of 5% in the range $z \leqslant 0.24$.

3.3 Uncertainty of the Analysis

We now consider the uncertainties in our analysis. The errors are divided into three components: uncertainty due to the light curve fitting (including observational photometric errors), uncertainty due to the K-correction, and uncertainty due to the cosmological parameters adopted.

We estimated the uncertainty due to the light curve fitting with Monte Carlo simulations. We created artificial light curves from the light curve template based on the observed dates and photometric errors of each epoch. We measured the dispersion of each fitting parameter (luminosity, stretch factor, and time), and estimated the size of error. The typical errors in estimating luminosity at $z = 0.2$ are ~ 0.4 mag in *U*-band, ~ 0.05 mag in *B-, V-* and *R*-band, and ~ 0.2 mag in *I*-band. The typical errors in estimating stretch factors at $z = 0.2$ are ~ 0.3 in *U*-band, ~ 0.07 in *B-* and *V*-band, ~ 0.1 in *R*-band, and ~ 0.3 in *I*-band.

It is difficult to estimate the uncertainty due to the K-correction. As described above, we applied Hsiao's template to all SNe Ia in our sample, some SNe in our sample might include SNe Ia which have spectra which differ from Hsiao's

Table 3. Relations between B-band stretch factor and stretch factors in U- and V-band of the Nearby SNe Ia from TAK08

Relation	r.m.s.	Number
$s_{(U)} = (0.95 \pm 0.02) \times s_{(B)} + (0.16 \pm 0.02)$	0.09	75
$s_{(V)} = (0.88 \pm 0.01) \times s_{(B)} + (0.16 \pm 0.01)$	0.08	92

template. If one particular SN Ia has a spectrum which differs strongly from Hsiao's template, for example, like that of SN1991T or SN1991bg, we might significantly overestimate or underestimate the size of K-correction. For example, we show the value of K-correction at B-band maximum versus redshift in the top panel of Figure 4. As is clear in the figure, the difference is significantly larger than the errors due to light curve fitting. We remove those outliers based on the chi square probability of light curve fitting. The 643 SNe Ia used in this paper do not contain outliers.

If the SN Ia has a spectrum similar to that of Hsiao's template, the typical error in K-correction is 0.01 to 0.02 mag in the range $z < 1.0$ from SNLS study (Foley et al. 2008b). We also compared the difference between Hsiao's template and Nugent's template "Branch Normal" (in the bottom panel of Figure 4), and confirmed the difference is negligible (the size is only $\leqslant 0.005$ mag in U- and B-band).

The uncertainty due to the cosmological parameters also affects our estimation of distance modulus (absolute magnitude). If H_0 moves 1σ ($+1.6$ and -1.5 km s^{-1}Mpc^{-1}, Spergel et al. 2007), the distance modulus changes by 0.04 mag. Adopting a slightly different value for H_0 only shifts the zeropoint of the absolute magnitude, and it does not affect the conclusions in this study. A change of 1σ in Ω_m and Ω_Λ is equivalent to only 0.002 mag of distance modulus at $z = 0.2$. Note that the uncertainty is negligible for the comparison of samples with the same redshift, but is important for the comparison of samples with different redshifts.

Any uncertainty in the redshift of an event creates a corresponding uncertainty in its distance modulus. The redshifts of all SNe Ia used in this study were measured by a host galaxy spectrum or a SN spectrum, with a typical uncertainty in redshift of 0.001; this corresponds to an uncertainty of 0.01 mag at $z = 0.2$.

The main component of uncertainty is due to light curve fitting (see Table 4). In the following discussion, the errors of each parameter include all of uncertainties.

4 OBSERVATIONAL BIAS OF THE SDSS SAMPLE

In this section, we discuss the observational biases of the SDSS sample used in this study.

4.1 Selection Bias of the SDSS Sample

The most important case of selection biases in the SDSS sample is due to the detection limit of the SDSS 2.5-metre photometry in which the candidates are identified (see Figure 5). The signal-to-noise ratio (S/N) threshold for object detection is ~ 3.5, in typical conditions, corresponding to $g \sim 23.2, r \sim 22.8$, and $i \sim 21.2$ mag in AB system (Dilday et al. 2008). From Monte-Carlo simulations with artificial SNe, Dilday et al. (2008) showed the survey efficiency is 100% for candidates whose g-band maximum brightness is brighter than ~ 21.2 mag.

Another aspect is the bias due to the SN search strategy, especially spectroscopic target selection (Sako et al. 2008). Since the survey typically found 10 SN candidates per night, they could not all be observed spectroscopically. We chose targets for spectroscopic observations based on their probability of being SNe Ia. The likelihood was calculated from g-, r- and i-band light curve fitting with four parameters, z, A_{Vsdss}, T_{max}, and a *template*; here A_{Vsdss} is the host galaxy extinction in V-band under the assumption that $R_V = 3.1$, T_{max} is the time of rest-frame B-band maximum light, and the *template* is taken from a set of seven light curves, of SNe type Ia (normal, SN1991T-like, and SN1991bg-like), Ib, Ic, II-P and II-L SNe. We searched for best fit parameters for each candidate, and ranked them by the probability of being SNe Ia. Many SNe Ia were undoubtedly lost with lower priorities, especially since at high redshift the detected candidates increase in proportion to the survey volume while the number of spectroscopically observed SNe Ia decreases. Type-119 and 120 SNe are strongly affected by the bias, and type-105 SNe are also affected by the bias since the probability of being a SN Ia is calculated based on the same fitting parameters given here. The possible missed SNe Ia are (1) obscured SNe Ia, (2) SNe Ia which occurred in the centre of the host galaxy, and (3) SNe Ia with peculiar light curves.

4.2 Contamination of other type SNe

As discussed in §2, we added type-105 SNe Ia to the SDSS sample in order to reduce the biases described above and to preserve the diversity of the sample since type-120 and 119 SNe Ia are strongly biased (Sako et al. 2011). However, the incorporation of type-105 events may introduce contamination by other types of SNe. According to spectroscopic observations of SN Ia candidates which correspond to type-105, the probability of misidentification is about 10% (Dilday et al. 2008). Since the SN candidates were selected based only on photometry at early phases, the probability of misidentification would be smaller than 10% for the type-105 SNe Ia with late epoch observations. So the number of those misidentified SN must be less than 8 in the range $z < 0.24$ (we have 75 type-105 SNe Ia at the redshift range). In the following discussion, we use type-105 SNe Ia as well as type-120 SNe Ia.

Table 4. Typical errors in estimating luminosity and stretch factors at $z = 0.2$.

	σ_{M_B}	s.f.	Comment
Light Curve Fitting	0.05	0.06	including photometric errors of each epoch
K-correction	0.02	-	Branch Normal SN Ia only, Foley et al. (2008a)
Cosmological Parameters	0.002	-	
Redshift Estimation	0.01	-	
Total	0.06	0.06	

5 RESULTS

5.1 Photometric Properties of SNe Ia

Our sample consists of 643 SNe. We did not exclude SNe Ia due to any properties such as spectroscopic subtypes or host galaxy types from the sample. Because of poor *u*- and *z*-band photometry relative to *g*-, *r*- and *i*-band, we do not use stretch factors and peak magnitudes of *u*- and *z*-band in this study (*u*-band corresponds to *U*-band in the range $z < 0.24$, and *z*-band corresponds to *I*-band in the range $z < 0.24$ and *R*-band in the range $z \geqslant 0.24$). Also, we do not use photometric data with large errors ($> 20\%$). After discarding events with inadequate photometry, we have 342 SNe Ia, which are used in the following discussion. All parameters of the 342 SNe Ia are given at the online table (partly given in Table 5).

5.1.1 Stretch Factor Distribution

The stretch factor is one of the simplest parameters reflecting intrinsic properties of SNe Ia among the parameters derived from light curve fitting since stretch factors are not affected by the host galaxy dust. In the lower right panel of Figure 6, we show the distribution of *B*-band stretch factor for the 342 SNe Ia in the range $z < 0.24$ which are expected to be least biased by observational selections. In this figure, we also show the stretch distributions of the Nearby SNe Ia used in TAK08, in which three major data sets were identified (Hamuy et al. 1996a; Riess et al. 1999; Jha et al. 2006, hereafter HAM96, RIE99, JHA06; 28 SNe Ia from HAM96, 20 SNe Ia from RIE99, 36 SNe Ia from JHA06).

The SNe Ia shown in RIE99 and JHA06 were not found in a systematic SN search program. Their SNe Ia were selected from the IAU's Central Bureau for Astronomical Telegrams (CBAT). On the other hand, the SNe Ia shown in HAM96 were discovered by the CALAN/TOLOLO Supernova Search (Hamuy et al. 1993), which is a repeated scan SN survey of galaxy clusters which include many early type galaxies. This fact may result in an excess of events with a lower stretch value in the HAM96 sample since early type galaxies tend to host lower stretch SNe Ia (c.f. Howell 2001; van den Bergh et al. 2005). The stretch distributions of RIE99 and JHA06 shown in Figure 6 seem to have fewer SNe Ia with small stretch values than those in HAM96; recall that SNe with small stretch values are expected to be fainter than average SNe Ia. This difference may be caused by observational selection biases since the samples made from the SNe Ia reported in CBAT are expected to include fewer less-luminous SNe Ia with narrower light curves.

In order to compare photometric properties of the SDSS SNe with different stretch factors, we classified the SDSS sample into three subsamples as follows. (1) "Narrow" : $s_{(B)} \leqslant 0.9$, (2) "Medium" : $0.9 < s_{(B)} \leqslant 1.1$, and (3) "Broad" : $s_{(B)} > 1.1$.

5.1.2 Stretch-Magnitude Relation

We compared the stretch-magnitude relations derived from the Nearby sample with those of the SDSS sample. Figure 7[1] shows the *B*- stretch-magnitude relation in different redshift bins. In the range $z \leqslant 0.24$, the distribution of the SDSS sample seems to be similar to the stretch-magnitude relation derived from the Nearby sample except for the SNe Ia with large inverse *B*-band stretch factor.

As shown in Figure 8, we define the *B*-band residual (hereafter ΔM_B) from the regression line of stretch-magnitude relation of the bluest SN sample, which is expected to be almost free from dust extinction. Figure 9 shows the histogram of ΔM_B of the SDSS sample using the stretch-magnitude relation derived from the Nearby sample in TAK08 ($M_B = 2.28 \times s_{(B)}^{-1} - 21.49$, see Table 6 in TAK08). The histograms have tails toward large ΔM_B possibly due to host galaxy dust extinction. However, the Narrow SNe Ia lack this asymmetry, and some of them are significantly more luminous than predicted by the stretch-magnitude relation.

5.1.3 Stretch-Colour Relation

We also compared the stretch-colour relation derived from the Nearby sample with that of the SDSS sample. In order to avoid significant reddening caused by host galaxy dust, we select SNe based on the $M_B - M_V$ colour at the *B*-band maximum date because *B*- and *V*-bands are the bands with the least dispersion among optical passbands (James et al. 2006). We find the blue end of the SDSS SNe Ia has the following value, with an error smaller than 0.05 mag.

$$(M_B - M_V)_{max} = -0.28 \times s_{(B)} + 0.22 \quad (2)$$

We select the SDSS SNe Ia whose observed $(M_B - M_V)_{max}$ colour is within a range of 0.05 mag of the value above as a sample of SNe Ia with low extinction (hereafter, the BV-selected SDSS sample, see Figure 10).

Figures 11 and 12 show the stretch-colour relations of the SDSS sample and the Nearby sample. The $(M_V - M_R)_{max}$ distribution of BV-selected SDSS SNe Ia, except a few outliers, is similar to that of the Nearby SNe Ia (see

[1] We use inverse *B*-band stretch factor in these figures for the comparison with Figure 16 in TAK08.

Table 5. The sample of the fitting parameters of the 342 intermediate redshift SDSS SNe Ia. Complete data are provided at online.

SDSS-SNID	SN name	Type	$s_{(B)}$	M_B	M_V	M_R	M_I
694	-	105	1.38(0.05)	-19.01(0.05)	-19.11(0.05)	-19.27(0.06)	-18.86(0.10)
722	SN2005ed	120	1.03(0.02)	-19.16(0.08)	-19.14(0.04)	-19.08(0.05)	-18.73(0.07)
744	SN2005ei	120	1.05(0.07)	-19.28(0.04)	-19.14(0.04)	-19.11(0.04)	-18.88(0.13)
762	SN2005eg	120	1.14(0.05)	-19.06(0.07)	-19.09(0.03)	-19.08(0.05)	-18.78(0.32)
774	SN2005ex	120	1.04(0.03)	-19.11(0.13)	-19.11(0.05)	-19.13(0.04)	-18.91(0.05)
1032	SN2005ez	120	0.74(0.03)	-18.54(0.11)	-18.61(0.05)	-18.74(0.04)	-18.89(0.16)
1241	SN2005ff	120	0.93(0.01)	-18.82(0.04)	-18.90(0.03)	-18.92(0.03)	-18.77(0.07)
1371	SN2005fh	120	1.09(0.02)	-19.58(0.04)	-19.49(0.03)	-19.46(0.04)	-19.28(0.06)
1395	-	105	1.00(0.06)	-18.96(0.10)	-18.95(0.06)	-19.12(0.06)	-18.92(0.16)
1415	-	105	1.12(0.08)	-18.73(0.07)	-19.00(0.05)	-19.02(0.06)	-19.28(0.20)
1525	-	105	1.73(0.08)	-18.49(0.05)	-18.37(0.02)	-18.73(0.03)	-18.57(0.03)
1595	-	105	1.00(0.05)	-19.32(0.07)	-19.27(0.06)	-19.33(0.05)	-19.14(0.17)
1686	-	119	0.90(0.07)	-18.00(0.12)	-18.22(0.09)	-18.24(0.09)	-18.30(0.13)
1740	-	105	0.94(0.05)	-18.97(0.08)	-18.96(0.03)	-19.03(0.04)	-18.96(0.16)
1794	SN2005fj	120	1.21(0.06)	-18.99(0.05)	-19.01(0.03)	-18.98(0.03)	-18.66(0.19)
2031	SN2005fm	120	1.08(0.04)	-19.49(0.03)	-19.43(0.03)	-19.34(0.06)	-19.15(0.08)
2057	-	105	1.01(0.06)	-18.81(0.09)	-19.08(0.11)	-19.10(0.18)	-18.78(0.34)
2102	SN2005fn	120	1.12(0.02)	-19.47(0.07)	-19.36(0.03)	-19.26(0.05)	-19.06(0.04)
2162	-	105	0.88(0.03)	-19.04(0.06)	-19.09(0.08)	-18.96(0.07)	-18.74(0.14)
2246	SN2005fy	120	1.03(0.07)	-18.74(0.13)	-18.87(0.08)	-18.96(0.10)	-18.69(0.28)
2308	SN2005ey	120	1.10(0.02)	-19.57(0.05)	-19.39(0.03)	-19.25(0.04)	-18.96(0.11)
2309	-	105	1.12(0.02)	-19.58(0.04)	-19.45(0.03)	-19.29(0.02)	-18.96(0.04)
2330	SN2005fp	120	0.76(0.09)	-18.24(0.09)	-18.31(0.11)	-18.39(0.09)	-18.48(0.33)
2372	SN2005ft	120	1.09(0.11)	-19.00(0.11)	-19.04(0.07)	-19.10(0.10)	-18.67(0.33)
2561	SN2005fv	120	1.01(0.01)	-18.80(0.03)	-18.89(0.03)	-18.94(0.03)	-18.81(0.08)
2635	SN2005fw	120	1.16(0.04)	-19.22(0.04)	-19.23(0.03)	-19.15(0.03)	-18.77(0.06)
2639	-	105	1.04(0.05)	-19.31(0.07)	-19.28(0.03)	-19.41(0.07)	-19.05(0.18)
2689	SN2005fa	120	1.13(0.03)	-19.09(0.04)	-19.15(0.03)	-19.26(0.03)	-19.06(0.11)
2734	-	105	1.15(0.07)	-18.35(0.10)	-18.45(0.05)	-18.55(0.14)	-18.45(0.20)
2916	SN2005fz	120	1.08(0.02)	-18.47(0.05)	-18.79(0.04)	-18.85(0.04)	-18.56(0.10)
2928	-	105	1.04(0.07)	-18.28(0.04)	-18.25(0.05)	-18.54(0.03)	-17.97(0.12)
2929	SN2005im	105	1.21(0.04)	-17.49(0.03)	-17.41(0.06)	-17.77(0.03)	-17.96(0.12)
2992	SN2005gp	120	0.91(0.02)	-18.73(0.05)	-18.88(0.03)	-19.00(0.03)	-18.62(0.14)
3049	-	105	1.01(0.05)	-19.26(0.17)	-19.07(0.09)	-19.12(0.04)	-18.59(0.13)
3080	SN2005ga	120	1.04(0.06)	-19.21(0.07)	-19.27(0.09)	-19.21(0.09)	-18.66(0.30)
3087	SN2005gc	120	1.07(0.02)	-19.09(0.03)	-19.14(0.03)	-19.17(0.04)	-18.78(0.14)
3256	SN2005hn	120	0.94(0.02)	-19.00(0.06)	-18.84(0.03)	-18.93(0.05)	-18.87(0.06)
3317	SN2005gd	120	0.97(0.03)	-18.96(0.04)	-19.00(0.03)	-19.12(0.04)	-18.79(0.14)
3331	SN2005ge	119	0.96(0.04)	-18.84(0.16)	-18.96(0.21)	-18.99(0.18)	-18.81(0.28)
3452	SN2005gg	120	1.07(0.02)	-19.36(0.04)	-19.26(0.04)	-19.21(0.05)	-19.03(0.15)
3488	-	105	0.97(0.08)	-18.24(0.07)	-18.41(0.13)	-18.70(0.12)	-18.37(0.19)
3508	-	105	1.01(0.07)	-16.49(0.14)	-17.32(0.14)	-17.23(0.14)	-17.49(0.24)
3592	SN2005gb	120	1.01(0.02)	-19.14(0.03)	-19.09(0.02)	-19.12(0.03)	-18.80(0.05)
3901	SN2005ho	120	1.14(0.01)	-19.18(0.03)	-19.21(0.02)	-19.26(0.02)	-19.00(0.03)
3959	-	105	0.98(0.09)	-17.95(0.10)	-18.30(0.23)	-18.41(0.24)	-18.82(0.39)
4019	-	105	1.03(0.02)	-18.63(0.09)	-18.76(0.06)	-18.92(0.04)	-18.83(0.16)
4064	-	119	0.85(0.03)	-18.93(0.07)	-19.03(0.06)	-18.89(0.03)	-19.10(0.06)
4065	-	105	0.98(0.03)	-19.28(0.04)	-19.25(0.04)	-19.23(0.04)	-18.95(0.08)
4281	SN2005in	105	0.97(0.03)	-19.48(0.06)	-19.46(0.09)	-19.39(0.05)	-19.20(0.09)
5339	-	105	1.07(0.07)	-17.71(0.11)	-18.56(0.08)	-18.71(0.05)	-18.85(0.07)

Peak magnitudes are shown in Vega system. Redshift of the SNe Ia will be published in Sako et al. (in prep).

Figure 11). Broad SNe Ia tend to be bluer in $(M_V - M_R)_{max}$ colour. The $(M_U - M_B)_{max}$ distribution of the BV-selected SDSS SNe Ia is also similar to that of the Nearby SNe Ia (see Figure 12). Broad SNe Ia also tend to be bluer in $(M_U - M_B)_{max}$ colour. The results that SNe Ia with large light curve width is blue are consistent with previous works (Phillips 1993; Riess et al. 1996).

5.2 Photometric Properties of Host Galaxies

5.2.1 Extinction Law of Host Galaxy Dust

It is important to correct for dust extinction in the host galaxy before making distance estimates using SNe. In particular, we must know the shape of extinction curve (colour-colour relation, the ratio of R_Y/R_X) and the zeropoint of

Table 6. Relations between ΔM_B and colour excess from the stretch-colour relation under different assumptions. $\sigma(mag)$ is root mean square (rms) of residuals from the relation in B-band and R_V is conversion factor of V-band translated from R_B.

Sample	Relation	$\sigma(mag)$	R_V	Number	Figure
All	$(0.24 \pm 0.02) \times \Delta M_B + (0.06 \pm 0.01)$	0.12	$3.2^{+0.3}_{-0.2}$	342	14
Broad	$(0.25 \pm 0.16) \times \Delta M_B + (0.07 \pm 0.07)$	0.18	$3.1^{+5.4}_{-1.2}$	41	17
Medium	$(0.28 \pm 0.03) \times \Delta M_B + (0.05 \pm 0.01)$	0.10	$2.7^{+0.4}_{-0.2}$	216	16
Narrow	$(0.33 \pm 0.18) \times \Delta M_B + (0.10 \pm 0.03)$	0.13	$2.3^{+2.8}_{-0.8}$	85	18

the extinction curve (magnitude-colour relation, the absolute value of R_X).

If the stretch-magnitude relation of the SDSS sample and the Nearby sample is the same, the residuals from the stretch-magnitude relation are mainly due to host galaxy dust extinction. Figure 13 shows the relation between $(M_B - M_V)_{max}$ and other colours. The direction of the arrows shows the shape of the extinction curves of dust in these host galaxies. It is similar to that of dust in the Milky Way ($R_V = 3.3$).

Figure 14 shows the ΔM_B and colour excess relation (hereafter, the ΔM_B-E relation) of the SDSS sample in the range $z < 0.24$. In the figure, we assume that the B-band residuals from the stretch-magnitude relation (ΔM_B) are due to extinction by host galaxy dust, and that colour excesses $E(B-V)_{obs}$ from the stretch-colour relation (eq.(2)) are due to reddening by host galaxy dust and a zeropoint offset. Figure 15 is the ΔM_B-E relation under a different stretch-magnitude relation ($M_B = 1.83 \times s_{(B)}^{-1} - 21.04$, which is equivalent to the relation shown in Altavilla et al. 2004; see details in TAK08). Figure 16 shows the ΔM_B-E relation of the Medium SDSS sample ($0.9 < s_{(B)} \leqslant 1.1$) in the range $z < 0.24$. Figures 17 and 18 are the same figures for the Broad SDSS sample and the Narrow SDSS sample. We discuss the possibility that there are different stretch-colour relations for the SNe Ia with different stretch factors in §6. The relations and conversion factors we derive are shown in Table 6.

5.2.2 Relations between SNe Ia and Host Galaxy Colour

We investigated relationships between the photometric properties of SNe Ia and their host galaxy types. Using the galaxies brighter than $g' = 21$ in the SDSS imaging data, Strateva et al. (2001) found that 90% of spectroscopically classified late-type galaxies have colour bluer than $u' - r' = 2.5$ and found no examples of spectroscopically classified early-type galaxies with colour bluer than $u' - r' = 2.05$. Based on the $u - r$ colour, we classified the SDSS SNe Ia into three subgroups as follows. (1) "Blue Host" : $u - r < 2.0$ corresponding to late types (Sb, Sc, and Irr), (2) "Red Host" : $u - r > 2.5$ corresponding to early types (E/S0 and Sa), and (3) intermediate colour : $2.0 \leqslant u - r \leqslant 2.5$. We show the relation between SNe Ia and host galaxy type in Figure 16, 17, 18 and 19.

Figures 16 and 18 show that the SNe Ia which appeared in the "Red Hosts" have smaller dispersion in colour excess around the best fit relation than that of the SNe Ia which appeared in the "Blue Hosts" (see Table 7). In addition, the Medium and Narrow SNe Ia which appeared in the "Red Hosts" have smaller ΔM_B, due to less extinction by the host galaxy dust (most have $\Delta M_B \sim 0.0$ mag), than that of the SNe Ia which appeared in the "Blue Hosts". On the other hand, the Broad SNe Ia which appeared in the "Red Hosts" have larger extinction ($\Delta M_B \sim 0.6$ mag, see Figure 17). Table 7 also shows that the dispersion in colour excess around the best fit relation is smaller in each SN Ia sample with $\Delta M_B < 0.5$ mag (7B).

6 DISCUSSION

As shown in §5.1, stretch-magnitude relations and stretch-colour relations of the SDSS sample in the range $z < 0.24$ are similar to those of the Nearby sample, and the result is consistent with other observational studies of SNe Ia at higher redshift (Riess et al. 1999; Garnavich et al. 2004; Riess et al. 2007; Bronder et al. 2008; Foley et al. 2008a). Since the SDSS SNe Ia sample is more homogeneous than any other large sample of SNe Ia made from surveys at lower redshift, the photometric properties derived in this work can be used as standard photometric properties of SNe Ia. Hence, it is worth reviewing photometric properties of SDSS SNe Ia in detail.

In particular, the ΔM_B-E relation is quite interesting (Figure 14). The dispersion around the ΔM_B-E relation might be consistent with the uncertainties (see Table 4) under the two assumptions that (1) peak luminosities and colours are the same for all SNe Ia after the stretch correction, and (2) extinction laws of dust in host galaxies are the same. However, the dispersion appears to be larger than the typical uncertainty (σ in colour is 0.08 mag at $z = 0.2$). This implies that the assumptions may be too simplified. We now discuss the possible diversity of photometric properties of SNe Ia and properties of dust extinction in their host galaxies.

6.1 Diversity of Photometric Properties of SNe Ia

Table 7 shows that the SNe Ia which appeared in the "Red Hosts" tend to have narrower light curves (30 / 216 SNe of the Medium sample and 18 / 85 SNe of the Narrow sample have "Red Hosts"; see also the ratio of red triangles to others in Figures 17 and 18). Since many of "Red Hosts" are early type galaxies, the tendency that the "Red Hosts" SNe Ia have a narrower light curve is consistent with previous studies (c.f. Hamuy et al. 1996b, 2000; Howell 2001; van den Bergh et al. 2005; Sullivan et al. 2006). The SNe Ia which

Table 7. Dispersion of $E(B-V)_0$ around the relations of ΔM_B and colour excess. See also Figure 19.

Sample		Red Host		Blue Host		All	
		$\sigma(mag)$	Number	$\sigma(mag)$	Number	$\sigma(mag)$	Number
Broad	7A	-	3	0.17	35	0.18	41
	7B	-	1	0.04	15	0.04	16
Medium	7A	0.10	30	0.10	160	0.10	216
	7B	0.09	26	0.09	135	0.08	183
Narrow	7A	0.10	18	0.14	53	0.13	85
	7B	0.05[a]	16	0.14	49	0.12	79
Total			51		248		342

7A is all of SNe of the subgroup.
7B is SNe with $\Delta M_B < 0.5$ mag.
a: One outlier is excluded.

appeared in the "Blue Hosts", however, have a variety of light curve widths. These observational results can be explained by postulating that the progenitors of SNe Ia which appeared in the "Red Hosts" are members of an old stellar population, but those of SNe Ia which appeared in the "Blue Hosts" belong to both old and young stellar populations. Some of SNe Ia which appeared in the "Red Hosts" have large ΔM_B (i.e. Figures 16 and 17). They can be explained if those "Red Hosts" are dusty red galaxies with large extinction. In fact, Strateva et al. (2001) reported about 10% (20/210) of late-type galaxies have a colour of $u'-r' > 2.5$. Also, based on inspections by eye, half of these very red host galaxies have morphologies of late-type galaxies.

The interpretation that there are two types of SNe Ia with different photometric properties, originating in young and old stellar populations, is consistent with the idea that there are two varieties of SNe Ia, named "tardy" and "prompt" (Mannucci et al. 2005). The SNe Ia which appear in the "Red Hosts" are all "tardy" SNe Ia and the SNe Ia which appear in the "Blue Hosts" are both "tardy" and "prompt" SNe Ia. Based on this idea, we can estimate the intrinsic dispersions of the "tardy" and "prompt" SNe Ia. The "B" samples in Table 7 show this dispersion to be 0.09 / 0.05 mag for the "tardy" SNe Ia ("Red Host" - "Medium / Narrow") and 0.04 mag for the "prompt" SNe Ia ("Blue Host" - "Broad").

Figure 20 shows the distributions of colour residuals from the expected colour of the Medium SNe Ia under the assumption that the dust properties are the same as those of the Galactic dust. The result of Kolmogorov-Smirnov test shows that the distributions of the Medium SNe Ia which appeared in the "Blue Hosts" and "Red Hosts" are different at a significance level 96.2%. These results support the possibility that there are two different populations of SNe Ia.

There is a possibility that large errors could mislead this analysis. However, the dispersion of colour residuals is significantly larger than the estimated uncertainty even if we select the Medium SNe Ia with smaller uncertainties ($\sigma_{M_B}, \sigma_{M_V} < 0.05$ mag, see Figure 21). There is another possibility that the two types of SNe Ia correspond to the Medium SNe Ia with larger $s_{(B)}$ and smaller $s_{(B)}$, because the $s_{(B)}$ range of the Medium SNe Ia is too wide to regard it as a homogeneous sample. However, the tendency is the same for the Medium SN Ia subsamples divided into four groups based on the B-band stretch factor ($0.90 \leqslant s_{(B)} < 0.95, 0.95 \leqslant s_{(B)} < 1.00, 1.00 \leqslant s_{(B)} < 1.05, 1.05 \leqslant s_{(B)} < 1.10$, see Figure 21). There is another possibility that the inverse stretch-magnitude relation ($M_B = 2.28 \times s_{(B)}^{-1} - 21.49$), which is used for deriving ΔM_B creates apparent two subgroups. However, we confirmed that there is no significant difference ($\sim 1\%$) between the Medium SN Ia subsamples based on the inverse and normal stretch-magnitude relation.

From these discussions, we conclude there may be two subgroups of Medium SNe Ia which have intrinsically different colours.

Sullivan et al. (2010) examined the colour-magnitude relation of the SNLS SNe sample. Although Figure 9 of Sullivan et al. (2010) shows basically the same properties as those in Figure 14, we cannot identify two distinct subgroups as in the Medium SDSS sample (Figure 16). Their results do not conflict with our findings since we cannot identify two subgroups in the SDSS sample which include the Narrow, Medium, and Broad SNe (Figure 14).

Lampeitl et al. (2010b) discussed the relation between properties of SN Ia and their host galaxies in the SDSS sample. They use the SALT2 (Guy et al. 2007) and the MLCS2k2 (Jha et al. 2007) for the parameterization of multi-band light curves, and found that introduction of the third parameter, a host galaxy type, reduces the luminosity dispersion after the corrections. Brandt et al. (2010) also found strong evidence of two progenitor channels related with the age of SN Ia progenitors from the delay time distribution of SDSS sample. These results are consistent with our conclusion that there are two subgroups of SNe Ia depending on the host galaxy colour.

6.2 Extinction Law of Host Galaxy Dust

Dust is another possible factor for creating large dispersions in the colour distributions of SNe Ia which appear in the "Blue Hosts" and "Red Hosts". As shown in Figure 13, the colour-colour relations derived from the SDSS sample in the range $z < 0.24$ indicate that the shape of extinction curves are similar to that of the Galactic dust. On the other hand,

the relations between ΔM_B and colour excess, which is related to the conversion factor R, have different implications.

From Figures 14 and 15, it is not clear whether or not the average R_V of host galaxy dust is close to the standard Galactic value ($R_V = 3.3$) . The value of R_V derived from the SDSS sample ($R_V = 3.2^{+0.3}_{-0.2}$) is similar to the standard Galactic value ("All" in Table 6).

However, as shown in §6.1, the SDSS sample may include two types of SNe Ia which have intrinsically different colours. In order to reduce the uncertainty of intrinsic diversity of SNe Ia colour, we derive R_V from the Medium, Broad and Narrow samples. Table 6 shows that average values of R_V of those three samples ("Broad", "Medium" and "Narrow" in Table 6) are smaller than the standard Galactic value. This result is consistent with previous studies (e.g. $R_B \sim 3.5$, Phillips et al. 1999; Knop et al. 2003; Altavilla et al. 2004; $R_B \sim 3.3$, Wang et al. 2006; $R_V = 1.75 \pm 0.27$, Nobili and Goobar 2008; $R_V = 2.2$, Kessler et al. 2010), which find values of R smaller than the standard Galactic value. In Figure 17, some of SNe Ia with large ΔM_B seem to be consistent with the standard Galactic value of R_V. This measurement may indicate that the value of R_V has a large intrinsic dispersion. In that case, in order to reduce uncertainty due to variety of R_V, we should use only the bluest SNe Ia for cosmological studies unless we know a proper R_V of each host galaxy. An example is given by Folatelli et al. (2010), who found $R_V \approx 1.7$ for their sample of SNe Ia, but this value changed to $R_V \approx 3.2$ if the highly reddened SNe are excluded.

In this study, SNe Ia which appeared in the "Blue Hosts" (see the blue squares in Figure 16) have a larger dispersion than that of the SNe Ia which appeared in the "Red Hosts", which are expected to be less affected by ISM. It is therefore difficult to explain the SNe Ia with large ΔM_B solely by extinction with small R_V. We conclude that the distributions shown in Figures 16 and 20 probably include a mixture of two factors, SNe Ia properties and dust properties.

6.3 Other factors which may have affected the observed SNe Ia colours

In the line of sight toward any SN Ia, there may be circumstellar dust (CSD) around the SN Ia in addition to dust in the interstellar medium (ISM). The existence of circumstellar material (CSM) is expected based on theoretical arguments (e.g. Nomoto 1982; Hachisu et al. 1999), and several recent observations have indicated the existence of circumstellar gas around spectroscopically normal SNe Ia (SN2000cx, Mazzali et al. 2005; Patat et al. 2007a; SN2003du, Germany et al. 2004; SN2005cg, Quimby et al. 2006; SN2006X, Patat et al. 2007b; SN2007af, Simon et al. 2007). Wang (2005) reported one possibility of CSD associated with circumstellar gas. The value of R_V from the "Red Hosts" is smaller than that of the Galactic ISM (see the distribution of red triangles in Figure 16). Smaller R values normally indicate a smaller size of dust particles (c.f. Draine 2003). Wang (2005) pointed out that a low R_V of host galaxy dust estimated from SNe Ia may be a result of the reflection effect from CSD.

New observations provide increasing number of evidence suggesting the presence of CSM/CSD in (at least some of) SNe Ia. Sternberg et al. (2011) showed that the sodium absorption features in 35 type-Ia SNe they observed indicate the presence of CSM around the progenitor system, which may have originated from gas outflows from the single-degenerate progenitors. Later, Dilday et al. (2012) reported a complex, multi-shell circumstellar material structure in the close environment of SN Ia PTF 11kx. An RS Oph-like symbiotic nova progenitor was proposed for this particular SN. Further, Förster et al. (2012, 2013) put forward new evidences for the presence and asymmetric distribution of CSM in SNe Ia from the observations of nearby SNe Ia. Also recently, Johansson et al. (2013) obtained strict upper limits for the amount of dust around three nearby SNe Ia down to $M_{dust} \lesssim 7 \times 10^{-3}$ $M_\odot$ with Herschel Space Observatory far-infrared observations, but could not completely rule out CSD as one contributor to the reddening suffered by SNe Ia.

Another possible factor affecting the observed SN Ia colour is the viewing angle of the asymmetric SN explosion. An off-center explosion of the white dwarf progenitor star in a SN Ia (Maeda et al. 2010) may affect the luminosity and colour of the SN (Maeda et al. 2011; Cartier et al. 2011). SNe viewed from the side closer to the ignition center will appear bluer, and those viewed from the other side will appear redder. The colour of the SN also seems to be correlated with the ejecta velocity (Foley & Kasen 2011; Foley 2012), with high-velocity SNe tend to be redder than the low-velocity ones.

While with the current photometric dataset we are unable to address the aforementioned points affecting the colours of our SNe, disregarding those possible factors we present the empirical result of our study as follows. A schematic picture of our conclusion based on the discussion above is shown in Figure 22. There may be two types of SNe Ia with different intrinsic colours, and their colours are affected by dust with different extinction properties.

7 SUMMARY

In this paper, we present photometric properties of the intermediate redshift SNe Ia found by SDSS-II SN Survey. The *u-, g-, r-, i-* and *z*-band light curves of the SDSS SNe Ia are parameterized into rest-frame *U-, B-, V-, R-* and *I*-band stretch factors, peak luminosities, and *B*-band maximum luminosity dates using the Multi-band Stretch Method. Considering the observational errors and selection biases, we select 342 SNe Ia in the range $z < 0.24$ for a study of their photometric properties. Stretch-magnitude and stretch-colour relations of the SDSS SNe Ia are similar to those of the Nearby SNe Ia. We find that most of the SNe Ia which appeared in the "Red Hosts" have a narrow light curve and the SNe Ia which appeared in the "Blue Hosts" have a variety of light curve widths. We infer that "tardy" SNe Ia appeared in both "Red Hosts" and "Blue Hosts" but "prompt" SNe Ia appeared in only "Blue Hosts", and find that both of them have a small dispersion (< 0.10 mag) in colour excess around the best fit relation. The Kolmogorov-Smirnov test shows that the colour distribution of the Medium SNe Ia depends upon host galaxy colour (significance level of 96.2%). These results indicate that there may be two types of SNe Ia with different intrinsic colours. We also discuss the dust

properties of host galaxies and find evidence that there may be dust with different extinction properties.

ACKNOWLEDGMENTS

Funding for the creation and distribution of the SDSS and SDSS-II has been provided by the Alfred P. Sloan Foundation, the Participating Institutions, the National Science Foundation, the U.S. Department of Energy, the National Aeronautics and Space Administration, the Japanese Monbukagakusho, the Max Planck Society, and the Higher Education Funding Council for England. The SDSS Web site is http://www.sdss.org/. This work was also supported in part by a JSPS core-to-core program "International Research Network for Dark Energy" and by a JSPS research grant (22012002).

The SDSS is managed by the Astrophysical Research Consortium for the Participating Institutions. The Participating Institutions are the American Museum of Natural History, Astrophysical Institute Potsdam, University of Basel, Cambridge University, Case Western Reserve University, University of Chicago, Drexel University, Fermilab, the Institute for Advanced Study, the Japan Participation Group, Johns Hopkins University, the Joint Institute for Nuclear Astrophysics, the Kavli Institute for Particle Astrophysics and Cosmology, the Korean Scientist Group, the Chinese Academy of Sciences (LAMOST), Los Alamos National Laboratory, the Max-Planck-Institute for Astronomy (MPA), the Max-Planck-Institute for Astrophysics (MPiA), New Mexico State University, Ohio State University, University of Pittsburgh, University of Portsmouth, Princeton University, the United States Naval Observatory, and the University of Washington.

This work is based in part on observations made at the following telescopes. The Hobby-Eberly Telescope (HET) is a joint project of the University of Texas at Austin, the Pennsylvania State University, Stanford University, Ludwig-Maximillians-Universität München, and Georg-August-Universität Göttingen. The HET is named in honor of its principal benefactors, William P. Hobby and Robert E. Eberly. The Marcario Low-Resolution Spectrograph is named for Mike Marcario of High Lonesome Optics, who fabricated several optical elements for the instrument but died before its completion; it is a joint project of the Hobby-Eberly Telescope partnership and the Instituto de Astronomía de la Universidad Nacional Autónoma de México. The Apache Point Observatory 3.5 m telescope is owned and operated by the Astrophysical Research Consortium. We thank the observatory director, Suzanne Hawley, and site manager, Bruce Gillespie, for their support of this project. The Subaru Telescope is operated by the National Astronomical Observatory of Japan. The William Herschel Telescope is operated by the Isaac Newton Group on the island of La Palma in the Spanish Observatorio del Roque de los Muchachos of the Instituto de Astrofisica de Canarias. The W. M. Keck Observatory is operated as a scientific partnership among the California Institute of Technology, the University of California, and the National Aeronautics and Space Administration. The Observatory was made possible by the generous financial support of the W. M. Keck Foundation.

We thank the SDSS collaborators for the discussions and meaningful suggestions for this work. We also thank Michael Richmond for carefully reading the manuscript.

REFERENCES

Aldering G., Adam G., Antilogus P., Astier P., Bacon R., Bongard S., Bonnaud C., Copin Y. et al., 2002, SPIE, 4836, 61

Altavilla G., Fiorentino G., Marconi M., Musella I., Cappellaro E., Barbon R., Benetti S., Pastorello A. et al., 2004, MNRAS, 349, 1344

Amanullah R., Lidman C., Rubin D., Aldering G., Astier P., Barbary K., Burns M. S., Conley A. et al., 2010, ApJ, 716, 712

Anderson, L., Aubourg, E., Bailey, S., et al. 2012, MNRAS, 427, 3435

Astier P., Guy J., Regnault N., Pain R., Aubourg E., Balam D., Basa S., Carlberg R. G. et al., 2006, A&A, 447, 31

Benetti S., Cappellaro E., Mazzali P. A., Turatto M., Altavilla G., Bufano F., Elias-Rosa N., Kotak R. et al., 2005, AJ, 623, 1011

Benson, B. A., de Haan, T., Dudley, J. P., et al. 2013, ApJ, 763, 147

Bildsten, L., Shen, K. J., Weinberg, N. N., & Nelemans, G. 2007, ApJL, 662, L95

Branch D., Fisher A., Nugent P., 1993, AJ, 106, 2383

Brandt, T. D., Tojeiro, R., Aubourg, É., et al. 2010, AJ, 140, 804

Bronder T. J., Hook I. M., Astier P., Balam D., Balland C., Basa S., Carlberg R. G., Conley A. et al., 2008, A&A, 477, 717

Campbell, H., D'Andrea, C. B., Nichol, R. C., et al. 2013, ApJ, 763, 88

Cardelli J. A., Clayton G. C., Mathis J. S., 1989, ApJ, 345, 245

Cartier, R., Förster, F., Coppi, P., et al. 2011, A&A, 534, L15

Conley, A., Guy, J., Sullivan, M., et al. 2011, ApJS, 192, 1

Dilday B. Kessler R., Frieman J. A., Holtzman J., Marriner J., Miknaitis G., Nichol R. C., Romani R. et al., 2008, ApJ, 682, 262

Dilday, B., Howell, D. A., Cenko, S. B., et al. 2012, Science, 337, 942

Doi M., Tanaka M., Fukugita M., Gunn J. E., Yasuda N., Ivezi$\hat{c}$ Ž., Brinkmann J., de Haars E. et al., 2010, AJ, 139, 1628

Draine B. T., 2003, ARA&A, 41, 241

Ellis R. S., Sullivan M., Nugent P. E., Howell D. A., Gal-Yam A., Astier P., Balam D., Balland C. et al., 2008, ApJ, 674, 51

Filippenko A. V., 1989, PASP, 101, 588

Filippenko A. V., Li W. D., Treffers R. R., 2001, ASPC, 246, 121

Filippenko A. V., 2005, ASSL, 332, 97

Folatelli, G., Phillips, M. M., Burns, C. R., et al. 2010, AJ, 139, 120

Foley R. J., Filippenko, A. V., Aguilera C., Becker A. C., Blondin S., Challis P., Clocchiatti A., Covarrubias R. et al., 2008, ApJ, 684, 68

Foley R. J., Filippenko A. V., Jha S. W., 2008, ApJ, 686, 117
Foley, R. J., & Kasen, D. 2011, ApJ, 729, 55
Foley, R. J. 2012, ApJ, 748, 127
Foley, R. J., Challis, P. J., Chornock, R., et al. 2013, ApJ, 767, 57
Förster, F., González-Gaitán, S., Anderson, J., et al. 2012, ApJL, 754, L21
Förster, F., González-Gaitán, S., Folatelli, G., & Morrell, N. 2013, arXiv:1304.6403 (ApJ accepted)
Frieman J. A., Bassett B., Becker A., Choi C., Cinabro D., DeJongh F., Depoy D. L., Dilday B. et al., 2008, AJ, 135, 338
Fukugita M., Ichikawa T., Gunn J. E., Doi M., Shimasaku K., Schneider D. P., 1996, AJ, 111, 1748
Galbany, L., Miquel, R., Östman, L., et al. 2012, ApJ, 755, 125
Garnavich P. M., Bonanos A. Z., Krisciunas K., Jha S., Kirshner R. P., Schlegel E. M., Challis P., Macri L. M. et al., 2004, ApJ, 613, 1120
Germany L. M., Reiss D. J., Schmidt B. P., Stubbs C. W., Suntzeff N. B., 2004, A&A, 415, 863
Gunn J. E., Carr M., Rockosi C., Sekiguchi M., Berry K., Elms B., de Haas E., Ivezić Ž. et al., 1998, AJ, 116, 3040
Gunn J. E., Siegmund W. A., Mannery E. J., Owen R. E., Hull C. L., Leger R. F., Carey L. N., Knapp G. R. et al., 2006, AJ, 131, 2332
Guy J., Astier P., Baumont S., Hardin D., Pain R., Regnault N., Basa S., Carlberg R. G. et al., 2007, A&A, 466, 11
Guy J., Sullivan M., Conley A., Regnault N., Astier P., Balland C., Basa S., Carlberg R. G. et al., 2010, A&A, 523A, 7
Hachisu I., Kato M., and Nomoto K., 1999, ApJ, 522, 487
Hamuy M., Phillips M. M., Wells L. A., and Maza, J. 1993, PASP, 105, 787
Hamuy M., Phillips M. M., Maza J., Suntzeff N. B., Schommer R. A., Aviles R., 1995, AJ, 109, 1
Hamuy M., Phillips M. M., Suntzeff N. B., Schommer R. A., Maza J., Antezan A. R., Wischnjewsky M., Valladares G. et al., 1996a, AJ, 112, 2408
Hamuy M., Phillips M. M., Suntzeff N. B., Schommer R. A., Maza J., Aviles R., 1996b, AJ, 112, 2391
Hamuy M., Trager S. C., Pinto P. A., Phillips M. M., Schommer R. A., Ivanov V., Suntzeff N. B., 2000, AJ, 120, 1479
Hamuy M., Folatelli G., Morrell N. I., Phillips M. M., Suntzeff N. B., Persson S. E., Roth M., Gonzalez S. et al., 2006, PASP, 118, 2
Hicken M., Challis P., Jha S., Kirshner R. P., Matheson T., Modjaz M., Rest A., Michael W. W. et al., 2009, ApJ, 700, 331
Hicken M., Wood-Vasey W. M., Blondin S., Challis P., Jha S., Kelly P. L., Rest A., Kirshner R. P., 2009, ApJ, 700, 1097
Holtzman J. A., Marriner J., Kessler R., Sako M., Dilday B., Frieman J. A., Schneider D. P., Bassett B. et al., 2008, AJ, 136, 2306
Howell D. A., 2001, ApJ, 554, L193
Hsiao E. Y., Conley A., Howell D. A., Sullivan M., Pritchet C. J., Carlberg R. G., Nugent P. E., Phillips M. M., 2007, ApJ, 663, 1187
Huterer D., Turner M. S., 1999, PhRvD, 60h, 1301
James J. B., Davis T. M., Schmidt B. P., Kim A. G., 2006, MNRAS, 370, 933
Jha S., Kirshner R. P., Challis P., Garnavich P. M., Matheson T., Soderberg A. M., Graves G. J. M., Hicken M. et al., 2006, AJ, 131, 527 (JHA06)
Jha S., Riess A. G., Kirshner R. P., 2007, ApJ, 659, 122
Johansson, J., Amanullah, R., & Goobar, A. 2013, MNRAS, 431, L43
Kelly P. L., Hicken M., Burke D. L., Mandel K. S., Kirshner R. P., 2010, ApJ, 715, 743
Kessler R., Becker A. C., Cinabro D., Vanderplas J., Frieman J. A., Marriner J., Davis T. M., Dilday B. et al., 2009, ApJS, 185, 32
Kessler R., Cinabro D., Bassett B., Dilday B., Frieman J. A., Garnavich P. M., Jha S., Marriner J. et al., 2010, ApJ, 717, 40
Knop R. A., Aldering G., Amanullah R., Astier P., Blanc G., Burns M. S., Conley A., Deustua S. E. et al., 2003, ApJ, 598, 102
Komatsu, E., Smith, K. M., Dunkley, J., et al. 2011, ApJS, 192, 18
Kowalski M., Rubin D., Aldering G., Agostinho R. J., Amadon A., Amanullah R., Balland C., Barbary K. et al., 2008, ApJ, 686, 749
Lampeitl H., Nichol R. C., Seo H.-J., Giannantonio T., Shapiro C., Bassett B., Percival W. J., Davis T. M. et al., 2010, MNRAS, 401, 2331
Lampeitl H., Smith M., Nichol R. C., Bassett B., Cinabro D., Dilday B., Foley R. J., Frieman J. A. et al., 2010, ApJ, 722, 566
Leibundgut B., Kirshner R. P., Phillips M. M., Wells L. A., Suntzeff N. B., Hamuy M., Schommer R. A., Walker A. R. et al., 1993, AJ, 105, 301
Li, H., Liu, J., Xia, J.-Q., et al. 2009, Physics Letters B, 675, 164
Malmquist K., 1920, Medd. Lund. Astron. Obs, 22, 1
Mannucci F., Della V. M., Panagia N., Cappellaro E., Cresci G., Maiolino R., Petrosian A., Turatto M., 2005, A&A, 433, 807
Mannucci F., Della V. M., Panagia N., 2006, MNRAS, 370, 773
Mazzali P. A., Benetti S., Altavilla G., Blanc G., Cappellaro E., Elias-Rosa N., Garavini G., Goobar A. et al., 2005, ApJ, 623L, 37
Maeda, K., Benetti, S., Stritzinger, M., et al. 2010, Nature, 466, 82
Maeda, K., Leloudas, G., Taubenberger, S., et al. 2011, MNRAS, 413, 3075
Neill J. D., Sullivan M., Howell D. A., Conley A., Seibert M., Martin D. C., Barlow T. A., Foster K. et al., 2009, ApJ, 707, 1449
Nobili S. and Goobar A., 2008, A&A, 487, 19
Nomoto K., 1982, ApJ, 253, 798
Nugent P., Phillips M., Baron E., Branch, D., Hauschildt P., 1995, ApJ, 455L, 147
Nugent P., Kim A., Perlmutter S., 2002, PASP, 114, 803
Oguri M., Inada N., Strauss M. A., Kochanek C. S., Richards G. T., Schneider D. P., Becker R. H., Fukugita M. et al., 2008, AJ, 135, 512
Oguri, M., Inada, N., Strauss, M. A., et al. 2012, AJ, 143, 120

Patat F., Benetti S., Justham S., Mazzali P. A., Pasquini L., Cappellaro E., Della Valle M., Podsiadlowski Ph. et al., 2007, A&A, 474, 931
Patat F., Chandra P., Chevalier R., Justham S., Podsiadlowski P., Wolf C., Gal-Yam A., Pasquini L. et al., 2007, Science, 317, 924
Percival W. J., Reid B. A., Eisenstein D. J., Bahcall N. A., Budavari T., Frieman J. A., Fukugita M., Gunn J. E. et al., 2010, MNRAS, 401, 2148
Perlmutter S., Aldering G., Goldhaber G., Knop R. A., Nugent P., Castro P. G., Deustua S., Fabbro S. et al., 1999, ApJ, 517, 565
Phillips M. M., Wells L. A., Suntzeff N. B., Hamuy M., Leibundgut B., Kirshner R. P., Foltz C. B., 1992, AJ, 103, 1632
Phillips M. M., 1993, ApJL, 413, 105L
Phillips M. M., Lira P., Suntzeff N. B., Schommer R. A., Hamuy M., Maza J., 1999, AJ, 118, 1766
Pignata, G., Maza, J., Hamuy, M., Antezana, R., & Gonzales, L. 2009, Revista Mexicana de Astronomia y Astrofisica Conference Series, 35, 317
Planck Collaboration, Ade, P. A. R., Aghanim, N., et al. 2013, arXiv:1303.5062
Pritchet C. J. and The SNLS Collaboration., 2005, ASP Confer. Ser. vol.334, Observing Dark Energy, ed. S. C. Wolff & T. R. Lauer, Astron. Soc. Pac., San Francisco, p. 60
Quimby R. M., Castro F., Gerardy C. L., Hoeflich, P., Kannappan S. J., Mondol P., Sellers M., Wheeler J. C., 2005, AAS, 20717102Q
Quimby R., Hoflich P., Kannappan S. J. et al., 2006, ApJ, 636, 400
Quimby R., Hoflich P., Wheeler J. C., 2007, ApJ, 666, 1083
Reid, B. A., Percival, W. J., Eisenstein, D. J., et al. 2010, MNRAS, 404, 60
Riess A. G., Press W. H., Kirshner R. P., 1996, ApJ, 473, 88
Riess A. G., Filippenko A. V., Challis P., Clocchiatti A., Diercks ., Garnavich P. M., Gilliland R. L., Hogan C. J. et al., 1998, AJ, 116, 1009
Riess A. G., Kirshner R. P., Schmidt B. P., Jha S., Challis P., Garnavich P. M., Esin A. A., Carpenter C. et al., 1999, AJ, 117, 707
Riess A. G., Strolger L-G., Tonry J., Casertano S., Ferguson H. C., Mobasher B., Challis P., Filippenko A. V. et al., 2004, ApJ, 607, 665
Riess A. G., Strolger, L.-G., Casertano S., Ferguson H. C., Mobasher B., Gold B., Challis P. J., Filippenko A. V. et al., 2007, ApJ, 659, 98
Sako M., Bassett B., Becker A., Cinabro D., DeJongh F., Depoy D. L., Dilday B., Doi M. et al., 2008, AJ, 135, 348
Sako M., Bassett B., Connolly B., Dilday B., Cambell H., Frieman J. A., Gladney L., Kessler R. et al., 2011, ApJ, 738, 162
Samushia, L., Reid, B. A., White, M., et al. 2013, MNRAS, 429, 1514
Scannapieco E., Bildsten L., 2005, ApJ, 629L, 85
Schlegel D. J., Finkbeiner D. P., Davis M., 1998, ApJ, 500, 525
Schmidt B. P., Suntzeff N. B., Phillips M. M., Schommer R. A., Clocchiatti A., Kirshner R. P., Garnavich P., Challis P. et al., 1998, ApJ, 507, 46
Simon J. D., Gal-Yam Avishay, Penprase B. E., Li Weidong, Quimby R. M., Silverman J. M., Allende P. Carlos, Wheeler J. C. et al., 2007, ApJ, 671L, 25
Smith, M., Nichol, R. C., Dilday, B., et al. 2012, ApJ, 755, 61
Spergel D. N., Bean R., Doré O., Nolta M. R., Bennett C. L., Dunkley J., Hinshaw G., Jarosik N. et al., 2007, ApJS, 170, 377
Sternberg, A., Gal-Yam, A., Simon, J. D., et al. 2011, Science, 333, 856
Strateva I., Ivezi$\hat{c}$ $\hat{Z}$., Knapp G. R., Narayanan V. K., Strauss, M. A., Gunn J. E., Lupton R. H., Schlegel D. et al., 2001, AJ, 122, 1861
Sullivan M., Le Borgne D., Pritchet C. J., Hodsman A., Neill J. D., Howell D. A., Carlberg R. G., Astier P. et al., 2006, ApJ, 648, 868
Sullivan M., Conley A., Howell D. A., Neill J. D., Astier P., Balland C., Basa S., Carlberg R. G. et al., 2010, MNRAS, tmp, 755
Suzuki, N., Rubin, D., Lidman, C., et al. 2012, ApJ, 746, 85
Takanashi N., Doi M., Yasuda N., 2008, MNRAS, 648, 868
Tegmark M., Eisenstein D. J., Strauss M. A., Weinberg D. H., Blanton M. R., Frieman J. A., Fukugita M., Gunn, J. E. et al., 2006, PhRvD, 74l3507T
Tonry J. L., Schmidt B. P., Barris B., Candia P., Challis P., Clocchiatti A., Coil A. L., Filippenko A. V. et al., 2003, ApJ, 594, 1
Turner M. S., 1999, AIPC, 478, 113T
van den Bergh S., Li W., Filippenko A. V., 2005, PASP, 117, 773
Wang L., 2005, AJ, 635, L33
Wang X., Wang L., Pain R., Zhou X., Li Z., 2006, ApJ, 645, 488
Wood-Vasey W. M., Miknaitis G., Stubbs C. W., Jha S., Riess A. G., Garnavich P. M., Kirshner R. P., Aguilera C. et al., 2007, ApJ, 666, 694
York D. G., Adelman J., Anderson J. E., Jr., A. S. F., Annis J., Bahcall N. A., Bakken J. A., Barkhouser R. et al., 2000, AJ, 120, 1579
Zheng C., Romani R. W., Sako M., Marriner J., Bassett B., Becker A., Choi C., Cinabro D. et al., 2008, AJ, 135, 1766

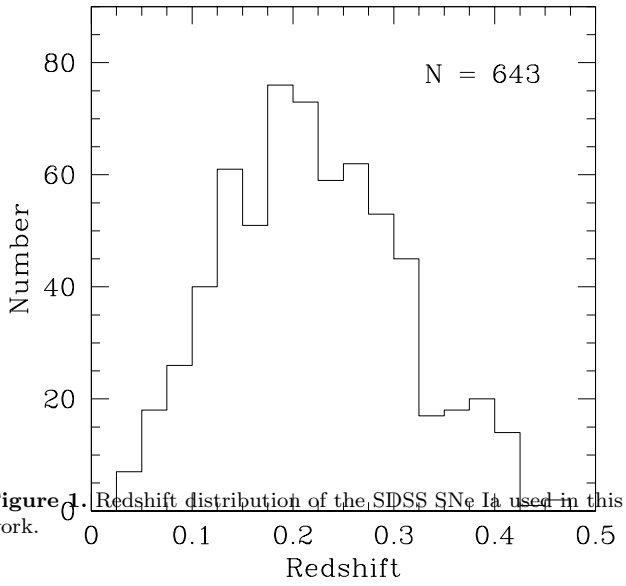

Figure 1. Redshift distribution of the SDSS SNe Ia used in this work.

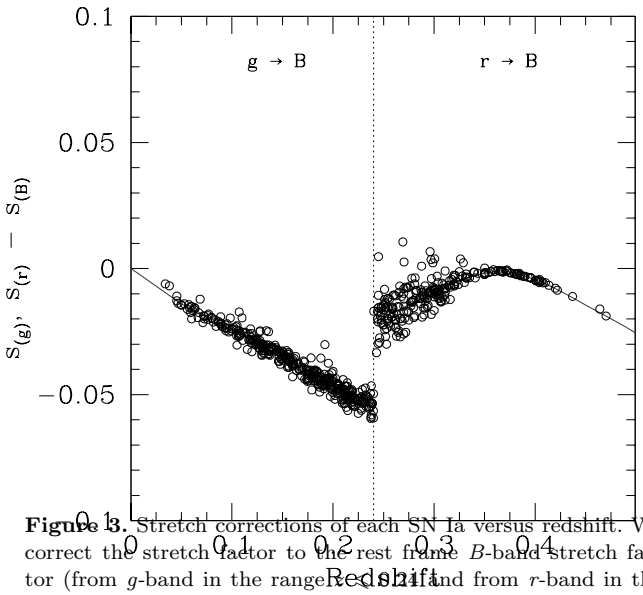

Figure 3. Stretch corrections of each SN Ia versus redshift. We correct the stretch factor to the rest frame B-band stretch factor (from g-band in the range $z \leqslant 0.24$ and from r-band in the range $0.24 < z \leqslant 0.50$). The solid line shows the size of stretch correction of SN Ia ($s_{(B)} = 1.0$). See text for description.

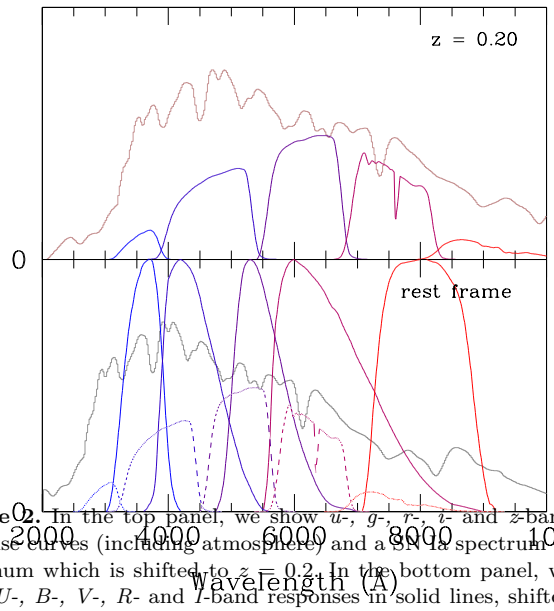

Figure 2. In the top panel, we show u-, g-, r-, i- and z-band response curves (including atmosphere) and a SN Ia spectrum at maximum which is shifted to $z = 0.2$. In the bottom panel, we show U-, B-, V-, R- and I-band responses in solid lines, shifted u-, g-, r-, i- and z-band response at $z = 0.2$ in dashed lines, and a rest frame SN Ia spectrum at maximum.

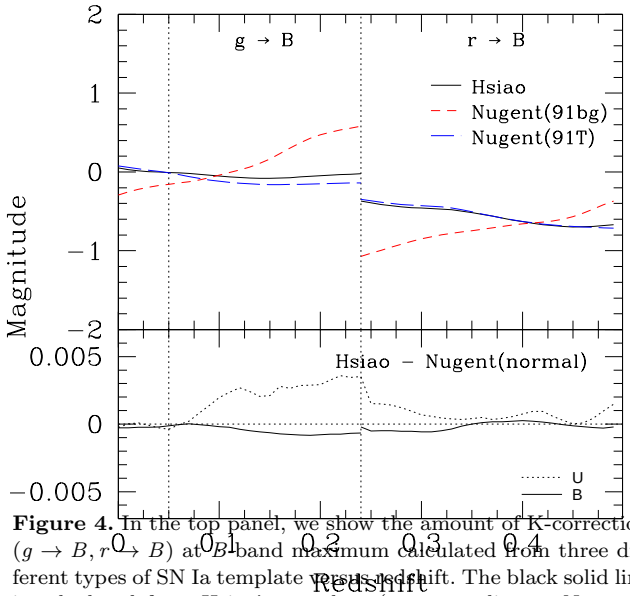

Figure 4. In the top panel, we show the amount of K-correction ($g \rightarrow B, r \rightarrow B$) at B-band maximum calculated from three different types of SN Ia template versus redshift. The black solid line is calculated from Hsiao's template (corresponding to Nugent's normal template), the short dashed red line is calculated from Nugent's SN1991bg-like template, and the long dashed red line is calculated from Nugent's SN1991T-like template. In the bottom panel, we show the difference between K-corrections which calculated from Hsiao's template and Nugent's Branch Normal template in U- and B-band versus redshift. Vertical dotted lines denote the border of band combinations for K-correction.

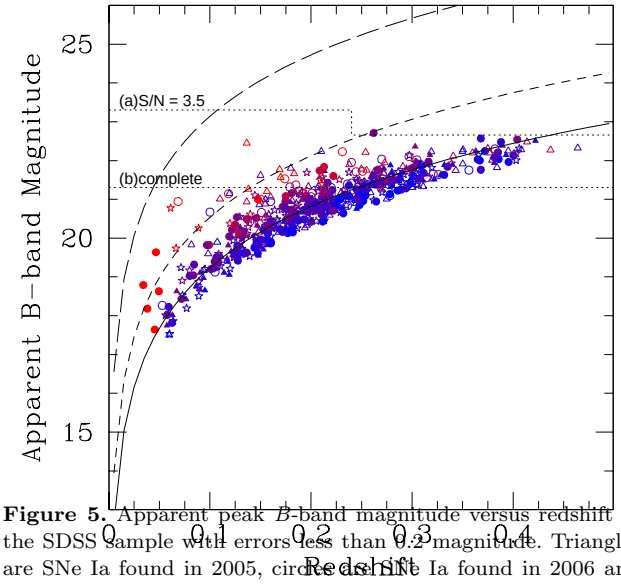

Figure 5. Apparent peak B-band magnitude versus redshift of the SDSS sample with errors less than 0.2 magnitude. Triangles are SNe Ia found in 2005, circles are SNe Ia found in 2006 and stars are SNe Ia found in 2007. Filled symbols are spectroscopically confirmed SNe Ia (type-120 and 118) and open symbols are spectroscopically or photometrically probable SNe Ia (type-119 and 105). The solid line denotes typical luminosity of SN Ia, -19.0 + distance modulus. The dotted lines denote (a) detection limit (S/N = 3.5) of the SDSS 2.5-metre telescope at APO and (b) complete limit estimated from Monte-Carlo simulation. The dashed lines denote the limits of host galaxy dust extinction parameter A_V (we transformed A_V to A_B in this figure); we set the value to 1.0 mag for the 2005 survey (short dashed line) and 3.0 mag for the 2006-2007 survey (long dashed line). The colour of the circles is related to $(M_B - M_V)_{max}$, the bluer SN Ia is coloured bluer and the redder SN is coloured redder. See also Sako et al. (2008).

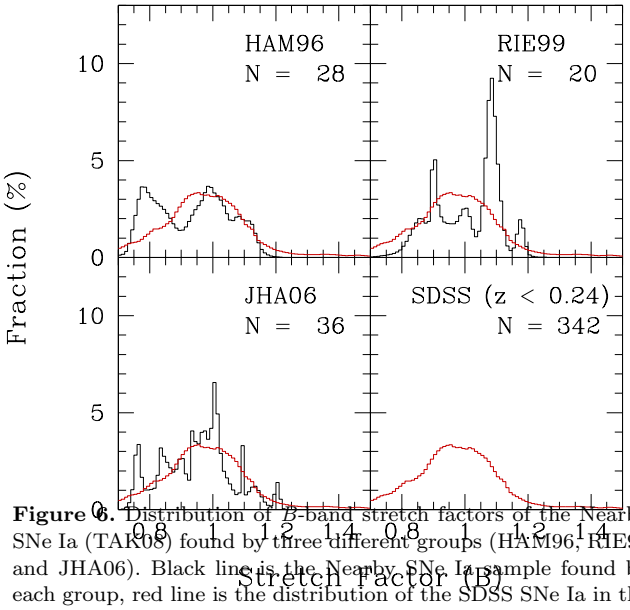

Figure 6. Distribution of B-band stretch factors of the Nearby SNe Ia (TAK08) found by three different groups (HAM96, RIE99 and JHA06). Black line is the Nearby SNe Ia sample found by each group, red line is the distribution of the SDSS SNe Ia in the range $z < 0.24$

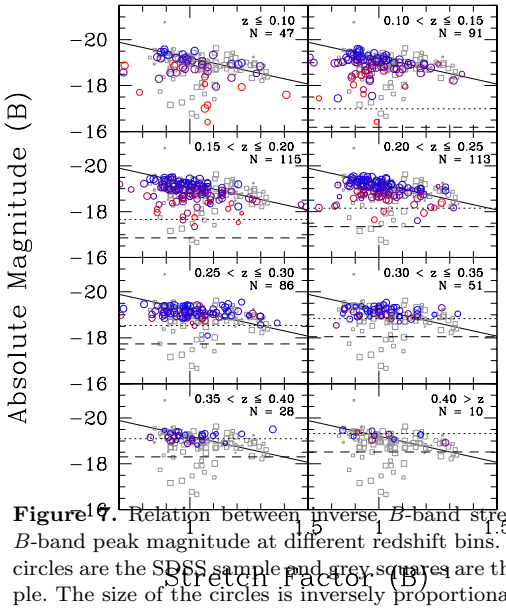

Figure 7. Relation between inverse B-band stretch factor and B-band peak magnitude at different redshift bins. Coloured open circles are the SDSS sample and grey squares are the Nearby sample. The size of the circles is inversely proportional to the size of errors, i.e. the larger the error estimation, the smaller the circle. The colour of the circles is related to $(M_B - M_V)_{max}$, the bluer SNe Ia are coloured bluer and the redder SNe Ia are coloured redder (same as Figure 5). The solid line denotes the relation between inverse B-band stretch factor and B-band magnitude derived from the Nearby sample in TAK08. The dotted lines denote 100% completeness limiting magnitude and the dashed lines denote 20% completeness limiting magnitude. SNe Ia with large errors ($\sigma_{M_B} > 0.2$) are excluded from this figure.

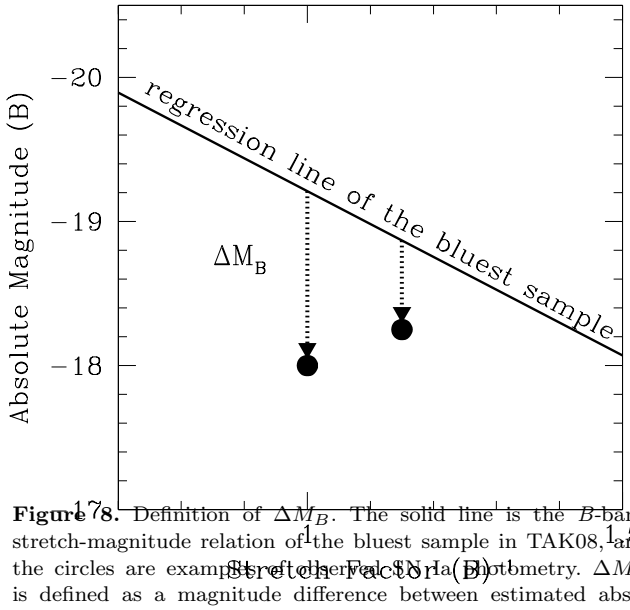

Figure 8. Definition of ΔM_B. The solid line is the B-band stretch-magnitude relation of the bluest sample in TAK08, and the circles are examples of observed SN Ia photometry. ΔM_B is defined as a magnitude difference between estimated absolute peak B-band magnitude from photometry and expected peak B-band magnitude from the B-band stretch-magnitude relation (shown by a dotted arrow). Positive ΔM_B indicates that a photometric point is below the regression line.

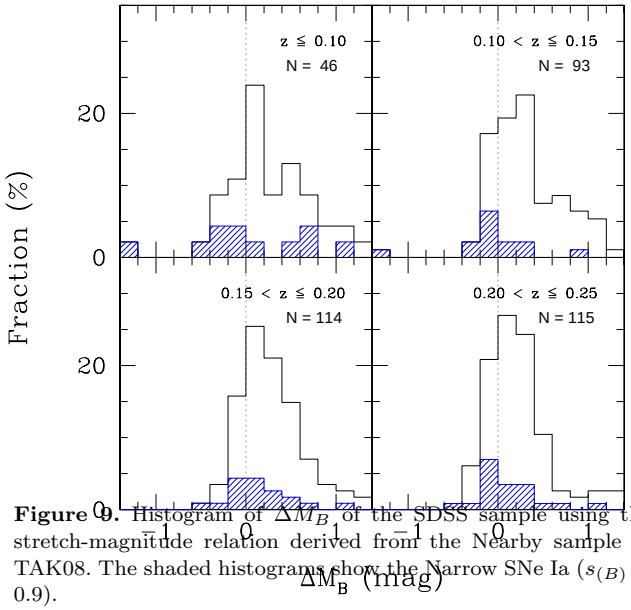

Figure 9. Histogram of ΔM_B of the SDSS sample using the stretch-magnitude relation derived from the Nearby sample in TAK08. The shaded histograms show the Narrow SNe Ia ($s_{(B)} < 0.9$).

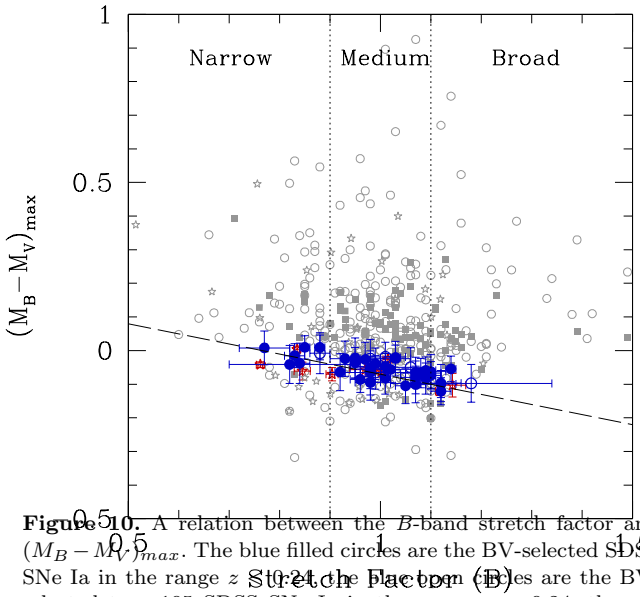

Figure 10. A relation between the B-band stretch factor and $(M_B - M_V)_{max}$. The blue filled circles are the BV-selected SDSS SNe Ia in the range $z < 0.24$, the Faint open circles are the BV-selected type-105 SDSS SNe Ia in the range $z < 0.24$, the red stars are the BV-selected Nearby SNe Ia, the filled grey squares are the SDSS SNe Ia with a smaller photometric error in the range $z < 0.24$, the grey stars are the other Nearby SNe Ia and the grey open circles are the others. The diagonal dashed line shows the blue end of the SDSS SNe Ia.

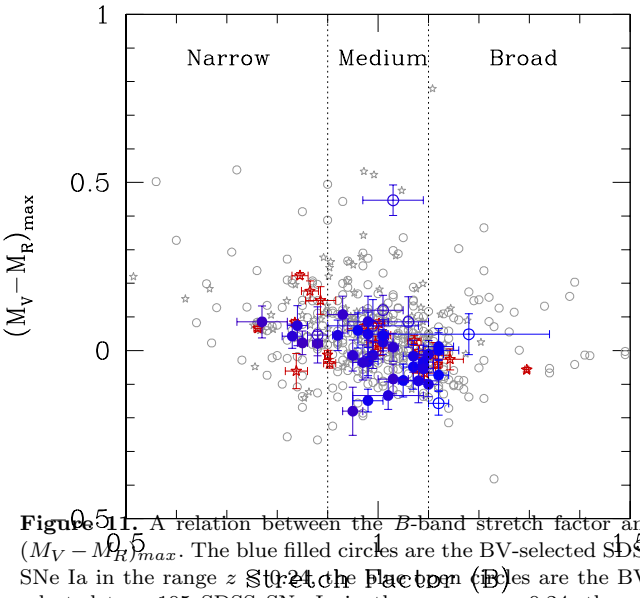

Figure 11. A relation between the B-band stretch factor and $(M_V - M_R)_{max}$. The blue filled circles are the BV-selected SDSS SNe Ia in the range $z < 0.24$, the Faint open circles are the BV-selected type-105 SDSS SNe Ia in the range $z < 0.24$, the red stars are the BV-selected Nearby SNe Ia, the grey stars are the other Nearby SNe Ia and the grey open circles are the others.

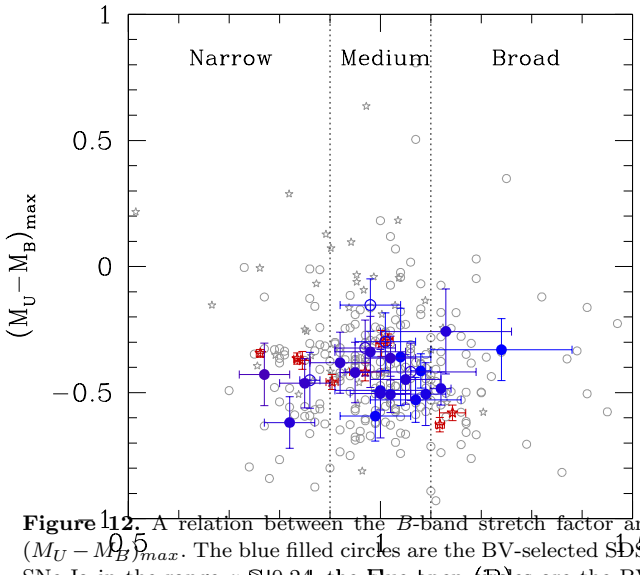

Figure 12. A relation between the B-band stretch factor and $(M_U - M_B)_{max}$. The blue filled circles are the BV-selected SDSS SNe Ia in the range $z \leqslant 0.24$, the blue open circles are the BV-selected type-105 SDSS SNe Ia in the range $z \geqslant 0.24$, the red stars are the BV-selected Nearby SNe Ia, the grey stars are the other Nearby SNe Ia and the grey open circles are the others.

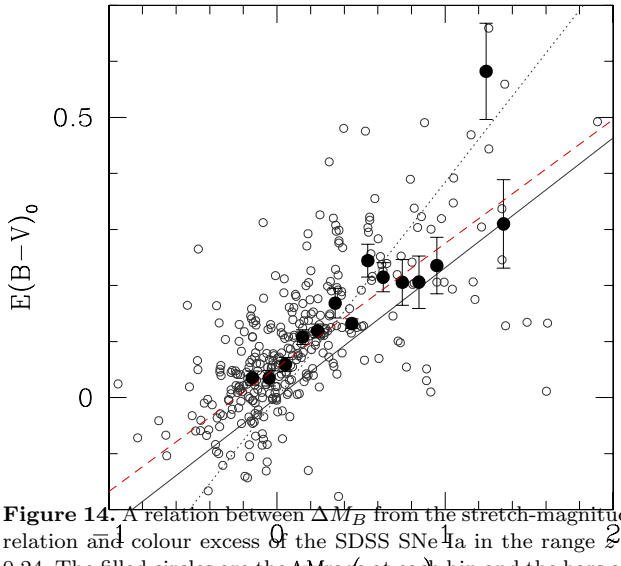

Figure 14. A relation between ΔM_B from the stretch-magnitude relation and colour excess of the SDSS SNe Ia in the range $z < 0.24$. The filled circles are the average in each bin and the bars are standard errors of the mean. The solid line denotes the conversion factor of standard Galactic extinction ($R_V = 3.3$), the dotted line denotes smaller conversion factor ($R_V = 2.0$), and the red dashed line is the best linear fit to the filled circle ($R_V = 3.2^{+0.3}_{-0.2}$).

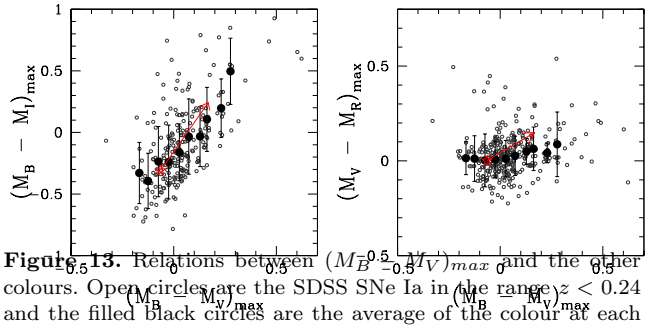

Figure 13. Relations between $(M_B - M_V)_{max}$ and the other colours. Open circles are the SDSS SNe Ia in the range $z < 0.24$ and the filled black circles are the average of the colour at each $(M_B - M_V)_{max}$ bin. The filled red stars denote the colour calculated from Hsiao's template and the red arrows denote the direction of extinction when we assume the value of conversion factor R is the same as that of the Milky Way (Schlegel et al. 1998, $R_V = 3.3$).

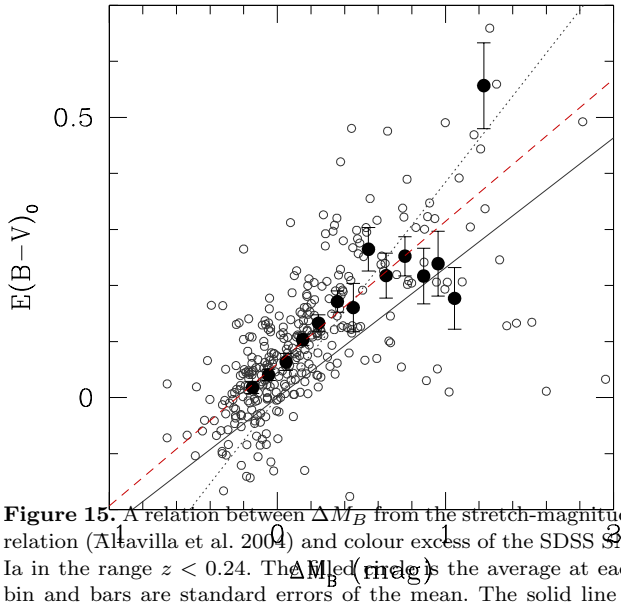

Figure 15. A relation between ΔM_B from the stretch-magnitude relation (Altavilla et al. 2004) and colour excess of the SDSS SNe Ia in the range $z < 0.24$. The filled circle is the average at each bin and bars are standard errors of the mean. The solid line is the conversion factor of standard Galactic extinction ($R_V = 3.3$), the dotted line denotes smaller conversion factor ($R_V = 2.0$), and the red dashed line is the best linear fit to the filled circle ($R_V = 3.2^{+0.1}_{-0.2}$).

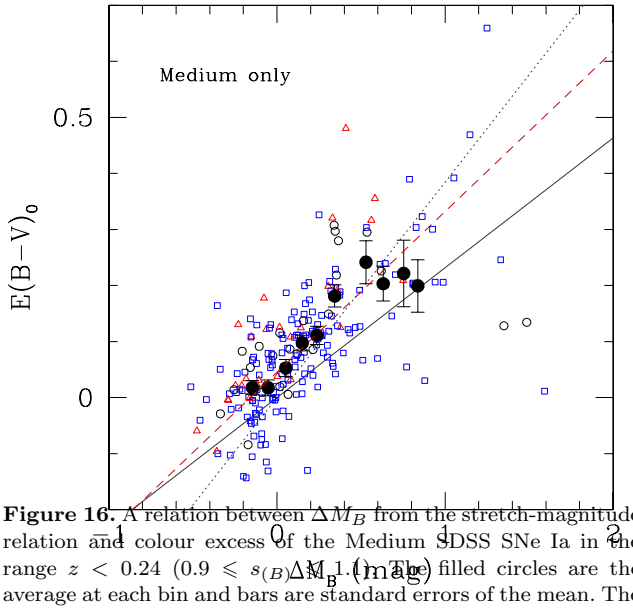

Figure 16. A relation between ΔM_B from the stretch-magnitude relation and colour excess of the Medium SDSS SNe Ia in the range $z < 0.24$ ($0.9 \leqslant s_{(B)} \leqslant 1.1$). The filled circles are the average at each bin and bars are standard errors of the mean. The blue squares show the SNe Ia which appeared in the "Blue Host" galaxies, the red triangles show the SNe Ia which appeared in the "Red Host" galaxies, and the black circles show the SNe Ia which appeared in the intermediate colour galaxies. The solid line is the conversion factor of standard Galactic extinction ($R_V = 3.3$), the dotted line denotes smaller conversion factor ($R_V = 2.0$), and the red dashed line is the best linear fit to the filled circle ($R_V = 2.7^{+0.4}_{-0.2}$).

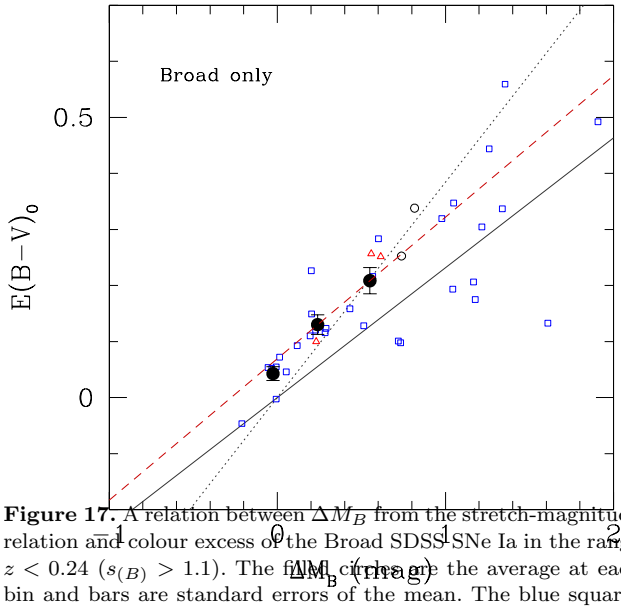

Figure 17. A relation between ΔM_B from the stretch-magnitude relation and colour excess of the Broad SDSS SNe Ia in the range $z < 0.24$ ($s_{(B)} > 1.1$). The filled circles are the average at each bin and bars are standard errors of the mean. The blue squares show the SNe Ia which appeared in the "Blue Host" galaxies, the red triangles show the SNe Ia which appeared in the "Red Host" galaxies, and the black circles show the SNe Ia which appeared in the intermediate colour galaxies. The solid line is the conversion factor of standard Galactic extinction ($R_V = 3.3$), the dotted line denotes smaller conversion factor ($R_V = 2.0$), and the red dashed line is the best linear fit to the filled circle ($R_V = 3.1^{+5.4}_{-1.2}$).

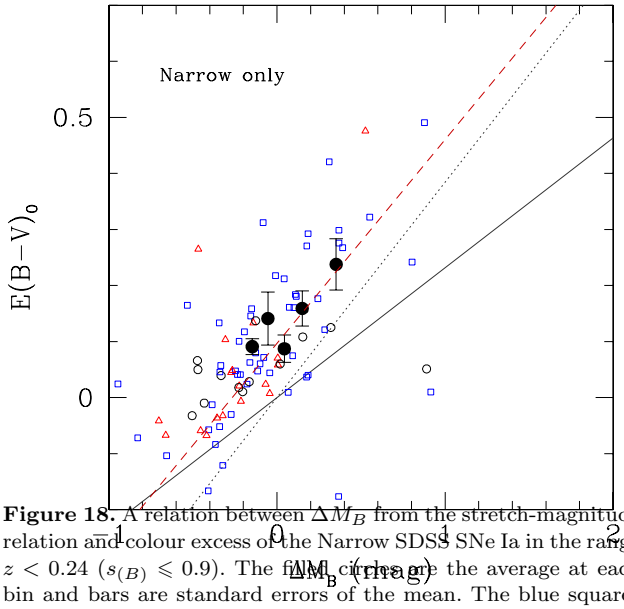

Figure 18. A relation between ΔM_B from the stretch-magnitude relation and colour excess of the Narrow SDSS SNe Ia in the range $z < 0.24$ ($s_{(B)} \leqslant 0.9$). The filled circles are the average at each bin and bars are standard errors of the mean. The blue squares show the SNe Ia which appeared in the "Blue Host" galaxies, the red triangles show the SNe Ia which appeared in the "Red Host" galaxies, and the black circles show the SNe Ia which appeared in the intermediate colour galaxies. The solid line is the conversion factor of standard Galactic extinction ($R_V = 3.3$), the dotted line denotes smaller conversion factor ($R_V = 2.0$), and the red dashed line is the best linear fit to the filled circle ($R_V = 2.3^{+2.8}_{-0.8}$).

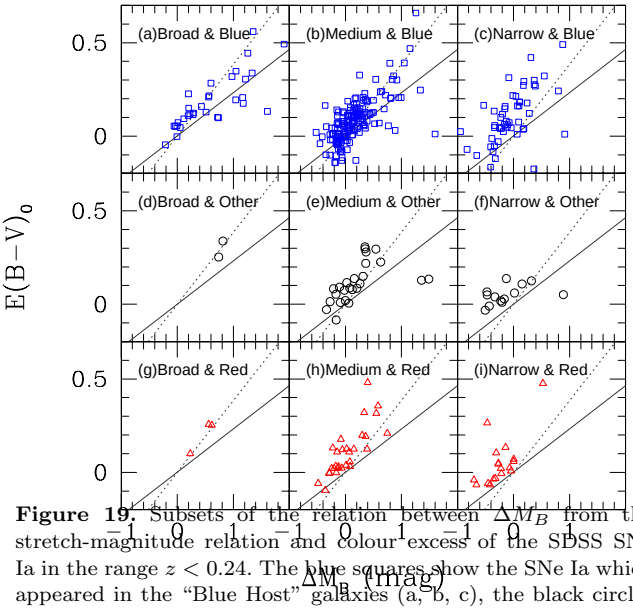

Figure 19. Subsets of the relation between ΔM_B from the stretch-magnitude relation and colour excess of the SDSS SNe Ia in the range $z < 0.24$. The blue squares show the SNe Ia which appeared in the "Blue Host" galaxies (a, b, c), the black circles show the SNe Ia which appeared in the intermediate colour galaxies (d, e, f), and the red triangles show the SNe Ia which appeared in the "Red Host" galaxies (g, h, i). They are also divided into three groups, Broad, Medium and Narrow. The solid line is the conversion factor of standard Galactic extinction ($R_V = 3.3$), and the dotted line denotes smaller conversion factor ($R_V = 2.0$).

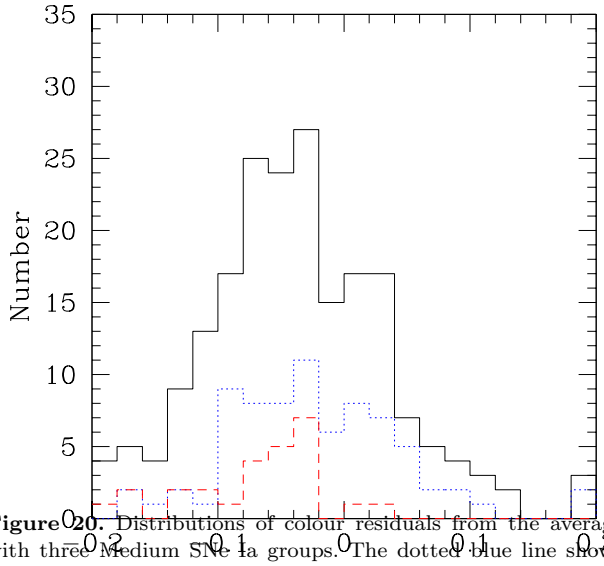

Figure 20. Distributions of colour residuals from the average with three Medium SNe Ia groups. The dotted blue line shows the "Blue Host" SNe Ia, dashed red line shows the "Red Host" SNe Ia, and the solid black line shows all of the Medium SNe Ia.

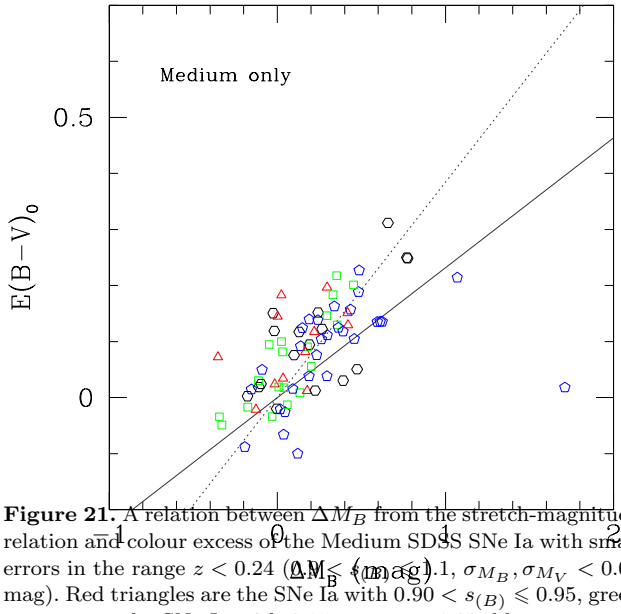

Figure 21. A relation between ΔM_B from the stretch-magnitude relation and colour excess of the Medium SDSS SNe Ia with small errors in the range $z < 0.24$ ($\Delta M_B < (\mathrm{mag}) < 0.1$, $\sigma_{M_B}, \sigma_{M_V} < 0.05$ mag). Red triangles are the SNe Ia with $0.90 < s_{(B)} \leqslant 0.95$, green squares are the SNe Ia with $0.95 < s_{(B)} \leqslant 1.00$, blue pentagons are the SNe Ia with $1.00 < s_{(B)} \leqslant 1.05$, and black sexanglulars are the SNe Ia with $1.05 < s_{(B)} \leqslant 1.10$. The solid line denotes the conversion factor of standard Galactic extinction ($R_V = 3.3$) and the dotted line denotes smaller conversion factor ($R_V = 2.0$).

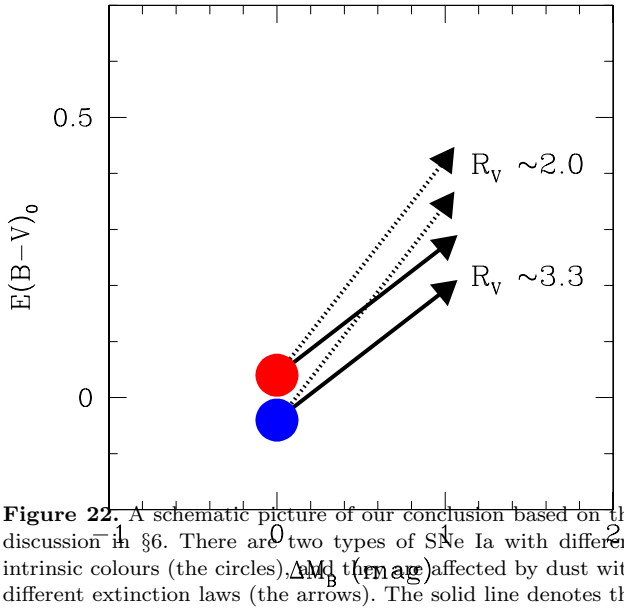

Figure 22. A schematic picture of our conclusion based on the discussion in §6. There are two types of SNe Ia with different intrinsic colours (the circles), and they are affected by dust with different extinction laws (the arrows). The solid line denotes the conversion factor of standard Galactic extinction ($R_V = 3.3$) and the dotted line denotes smaller conversion factor ($R_V = 2.0$). The distributions of SNe Ia shown in Figures 16 and 21 probably include a mixture of these factors.